

ON SUTURED FLOER HOMOLOGY AND THE EQUIVALENCE OF SEIFERT SURFACES

MATTHEW HEDDEN, ANDRÁS JUHÁSZ, SUCHARIT SARKAR

ABSTRACT. We study the sutured Floer homology invariants of the sutured manifold obtained by cutting a knot complement along a Seifert surface, R . We show that these invariants are finer than the “top term” of the knot Floer homology, which they contain. In particular, we use sutured Floer homology to distinguish two non-isotopic minimal genus Seifert surfaces for the knot 8_3 . A key ingredient for this technique is finding appropriate Heegaard diagrams for the sutured manifold associated to the complement of a Seifert surface.

1. INTRODUCTION

It is well-known that every knot in the three-sphere bounds an embedded orientable surface. The various surfaces which a given knot bounds are called *Seifert surfaces*, and play an important role in knot theory and low-dimensional topology as a whole. Given a knot, K , the minimum genus of any Seifert surface for K is called the *genus* of K . The genus of a knot is a fundamental invariant, and minimal genus Seifert surfaces tell us a lot about the topological and geometric properties of a knot. In particular, the only knot of genus zero is the unknot.

A natural question is to what extent minimal genus Seifert surfaces are unique. For instance, if a knot is fibered (that is, its complement is a fiber bundle over the circle with fibers consisting of Seifert surfaces) then the fiber surface is the unique minimal genus Seifert surface [2]. This means that any other minimal genus Seifert surface is isotopic to the fiber ¹. Many examples are known, however, of knots with non-isotopic Seifert surfaces [1, 3, 13, 14, 15, 17].

To date, most of the techniques for distinguishing Seifert surfaces have fallen into two categories: using the algebraic topology of the surface’s complement e.g. the fundamental group [1, 3, 17] or the Seifert form [30], and Gabai’s theory of sutured manifolds, [15, 13]. While the algebraic techniques are quite powerful, they often lead to difficult group or number theoretic questions and may be difficult to wield in general. Additionally, some examples are beyond the scope of traditional algebraic topological tools.

Sutured manifold theory, on the other hand, has provided methods - but not invariants - which have been useful in understanding minimal genus Seifert surfaces for many knots. The two techniques differ not only in spirit, but in the type of equivalence of Seifert surfaces which apply. Thus it would be desirable to have a computable invariant of Seifert surfaces which interacts well with the techniques of sutured manifold theory.

The purpose of this article is to show that *sutured Floer homology*, introduced by the second author in [10], is precisely such an invariant. Denoted $SFH(M, \gamma)$, the sutured Floer homology is an invariant associated to a (balanced) sutured manifold, (M, γ) , by a Lagrangian Floer homology construction.

Date: February 11, 2022.

1991 *Mathematics Subject Classification.* 57M27; 57R58.

¹There are two natural definitions of equivalence between Seifert surfaces, depending upon whether the isotopy occurs entirely in the complement. We review these subtleties in Section 4

Inspiration for the sutured Floer invariants came from the invariants of knots and three-manifolds defined by Ozsváth and Szabó [25, 24, 23, 27]. A key feature of the Ozsváth-Szabó invariants is their ability to detect the genus of a knot, K . The proof of this fact utilized sutured manifolds, but only so much as they were instrumental in providing taut foliations which allowed contact geometric and symplectic techniques to be employed [23].

With the advent of sutured Floer homology, a precise relationship between Gabai's machinery and Heegaard Floer homology has now been established [10, 11, 9]. Moreover, the genus detection of knot Floer homology has an elegant reinterpretation in this theory which we briefly explain.

Given a Seifert surface, R , for a knot $K \subset S^3$, we obtain a sutured manifold, $S^3(R) = (M, \gamma)$, by cutting along R . That is, we take $M = S^3 \setminus \text{Int}(R \times I)$ with suture $\gamma = \partial R \times I$. In [11] it was shown that

$$SFH(S^3(R)) \cong \widehat{HFK}(K, g(R)).$$

Here, the right hand side is the knot Floer homology group of K supported in Alexander grading $g(R)$ [24]. This isomorphism was then used, together with further properties of SFH and results of Gabai, to reprove (among many other things) the fact that knot Floer homology detects the genus. A striking aspect of this new proof is that it completely bypasses the four-dimensional methods which were originally used.

Now sutured Floer homology is an invariant of the sutured manifold, up to a natural notion of equivalence. It is immediate that isotopic Seifert surfaces produce equivalent sutured manifolds, and so one could hope that the sutured Floer homology of $S^3(R)$ provides interesting information about the isotopy type of R . This optimism is quickly challenged by the isomorphism above; the knot Floer homology groups do not depend on the Seifert surface. Examining the sutured Floer homology groups more closely, however, reveals structure not present in the knot Floer homology group. This additional structure takes the form of a grading by (relative) Spin^c structures.

For the reader unfamiliar with Spin^c structures, we recall that the space of Spin^c structures on a sutured manifold, (M, γ) , is isomorphic to $H_1(M; \mathbb{Z})$ as an affine space. Thus we can think of sutured Floer homology as having a grading by elements of $H_1(M; \mathbb{Z})$. Using this extra grading, we can provide the first explicit examples of minimal genus Seifert surfaces which are distinguished by sutured Floer homology. Indeed, we have the following theorem

Theorem 1.1. *There exist two minimal genus Seifert surfaces, R_1 and R_2 , for the knot 8_3 for which no isotopy of S^3 sends R_1 to R_2 . Indeed, there does not exist an orientation-preserving diffeomorphism of the pairs (S^3, R_1) , (S^3, R_2) .*

We remark that while it was previously known that R_1 and R_2 are not isotopic in the complement of 8_3 [15], the question of whether they were isotopic was open. Indeed, all previously available techniques fail to distinguish R_1 and R_2 , up to isotopy. See Subsection 4.1 for more details. Using the above example, we also obtain

Theorem 1.2. *For any $n \geq 1$, there exists a knot K_n with Seifert surfaces $\{F_0, \dots, F_n\}$, such that F_i is not isotopic to F_j for any $i \neq j$.*

Previously, there were examples known of knots possessing infinitely many Seifert surfaces which are pairwise non-isotopic in the complement of K [3]. However, these examples are known to be isotopic in S^3 , and again our theorem appears to be the strongest to date in the way of producing knots with many non-isotopic surfaces.

As the primary purpose of this article is to provide a foundation for further study, the details of any particular example are somewhat beside the point. We expect the techniques presented here to be applicable for a variety of questions in the study of Seifert surfaces, and conclude by briefly explaining the two major components of our framework.

The first is an explicit understanding of Heegaard diagrams for the sutured manifold associated to a Seifert surface. Section 3 discusses these diagrams in detail. In particular, we outline a very general method for obtaining such diagrams and then provide explicit algorithms.

The second key feature is the extraction of Spin^c information from the aforementioned diagrams. The difference between any two Spin^c structures supporting sutured Floer homology yields an element of $H_1(M; \mathbb{Z})$. This element can be explicitly identified from the Heegaard diagrams. However, it is difficult to determine whether $\gamma_1 \in H_1(M_1; \mathbb{Z})$, $\gamma_2 \in H_1(M_2; \mathbb{Z})$ presented by Heegaard diagrams for M_1 , M_2 , respectively, are identical (in the presence of an assumed equivalence between M_1 and M_2). In the present context, the key observation is that $H_1(S^3 \setminus R \times I; \mathbb{Z}) \cong H_1(R; \mathbb{Z})$. This isomorphism equips the former group with a bilinear form; namely, the Seifert form on R . We can use this form to distinguish elements of $H_1(S^3 \setminus R_i \times I)$ obtained as differences of Spin^c structures supporting non-trivial Floer homology. Distinguishing these elements, in turn, shows that the sutured manifolds are not equivalent and hence the Seifert surfaces are not isotopic. We find this second feature particularly interesting, as this is the first instance that the Seifert form has made any real appearance in the context of Heegaard Floer homology.

Acknowledgment: It is our pleasure to thank David Gabai, Chuck Livingston, and Zoltán Szabó for their interest in this work and many helpful conversations.

2. PRELIMINARIES

Sutured manifolds were introduced by Gabai in [4]. They provide a natural framework for constructing taut foliations on three-manifolds via inductive cut-and-paste procedures. The motivation for taut foliations, in turn, is that they tell us about the Thurston norm of three-manifolds [29]. In particular, they can be used to determine the genera of knots. Sutured Floer homology is a generalization of Ozsváth-Szabó Floer homology to an invariant of sutured manifolds, and was defined in [10]. Its definition and study were motivated by a desire to clarify and further explore connections between the Ozsváth-Szabó invariants and Gabai's theory hinted at by the results in [23]. In particular, a primary goal was to show that knot Floer homology detects fibered knots [8, 20, 11].

In this section, we begin by briefly recalling some basic notions from the theory of sutured manifolds. We then discuss sutured Floer homology, paying particular attention to sutured Heegaard diagrams. These diagrams are the input for the sutured Floer homology invariants. Special focus will be given to sutured Heegaard diagrams adapted to a decomposing surface and the way in which decomposition of sutured manifolds is understood in terms of these diagrams.

We refer the reader to [4, 5, 7] for more details on sutured manifolds, and to [10, 11] for details on sutured Floer homology.

2.1. Sutured Manifolds. The cornerstone of Gabai's machinery is the notion of a sutured manifold.

Definition 2.1. A *sutured manifold* (M, γ) is a compact oriented 3-manifold with boundary, $(M, \partial M)$, together with a set $\gamma \subset \partial M$ of pairwise disjoint annuli $A(\gamma)$ and tori $T(\gamma)$. Furthermore, the interior of each component of $A(\gamma)$ contains a *suture*, i.e., a homologically nontrivial oriented simple closed curve. We denote the union of the sutures by $s(\gamma)$.

Finally, every component of $R(\gamma) = \partial M \setminus \text{Int}(\gamma)$ is required to be oriented. Define $R_+(\gamma)$ (resp. $R_-(\gamma)$) to be those components of $\partial M \setminus \text{Int}(\gamma)$ whose normal vectors point out of (resp. into) M . The orientation on $R(\gamma)$ must be coherent with respect to $s(\gamma)$, i.e., if δ is a component of $\partial R(\gamma)$ and is given the boundary orientation, then δ must represent the same homology class in $H_1(\gamma)$ as some suture.

Definition 2.2. Two sutured manifolds $(M_1, \gamma_1), (M_2, \gamma_2)$ are said to be *equivalent* if there is an orientation-preserving diffeomorphism $f : M_1 \rightarrow M_2$ which restricts to an orientation-preserving diffeomorphism between $R(\gamma_1)$ and $R(\gamma_2)$.

Definition 2.3. A sutured manifold (M, γ) is called *balanced* if M has no closed components, $\chi(R_+(\gamma)) = \chi(R_-(\gamma))$, and the map $\pi_0(A(\gamma)) \rightarrow \pi_0(\partial M)$ is surjective.

The following two examples can be found in [6].

Example 2.4. Let R be a compact oriented surface with no closed components. Then there is an induced orientation on ∂R . Let $M = R \times I$, define $\gamma = \partial R \times I$, and finally put $s(\gamma) = \partial R \times \{1/2\}$. The balanced sutured manifold (M, γ) obtained by this construction is called a *product sutured manifold*.

Example 2.5. Let Y be a closed connected oriented 3-manifold and let $R \subset Y$ be a compact oriented surface with no closed components. We define a sutured manifold $Y(R) = (M, \gamma)$ to be the sutured manifold where $M = Y \setminus \text{Int}(R \times I)$, with the suture $\gamma = \partial R \times I$. Furthermore $s(\gamma) = \partial R \times \{1/2\}$.

From the perspective of Floer homology, the following example is also quite relevant.

Example 2.6. Let $K \subset Y$ be a knot, and let $Y_{2n}(K) = (M, \gamma_{2n})$ denote the sutured manifold with $M = Y \setminus \nu(K)$ the knot exterior, and $s(\gamma_{2n})$ consisting of $2n$ parallel copies of the meridian of K , with orientations alternating.

The key to Gabai's inductive procedures is the concept of a sutured manifold decomposition, which we now recall. See [4, Definition 3.1] and [7, Correction 0.3]. We begin with the notion of a decomposing surface.

Definition 2.7. Let (M, γ) be a sutured manifold. A *decomposing surface* is an oriented, properly-embedded surface, $S \subset M$, such that no component of ∂S bounds a disk in $R(\gamma)$ and no component of S is a disk D with $\partial D \subset R(\gamma)$. Moreover, for every component λ of $S \cap \gamma$ one of (1)-(3) holds:

- (1) λ is a properly-embedded non-separating arc in γ satisfying $|\lambda \cap s(\gamma)| = 1$.
- (2) λ is a simple closed curve in an annular component A of γ in the same homology class as $A \cap s(\gamma)$.
- (3) λ is a homotopically non-trivial curve in a torus component T of γ , and if δ is another component of $T \cap S$, then λ and δ represent the same homology class in $H_1(T)$.

A decomposing surface S defines a *sutured manifold decomposition*, denoted

$$(M, \gamma) \xrightarrow{S} (M', \gamma'),$$

where

$$\begin{aligned} M' &= M \setminus \text{Int}(N(S)), \\ \gamma' &= (\gamma \cap M') \cup N(S'_+ \cap R_-(\gamma)) \cup N(S'_- \cap R_+(\gamma)), \\ R_+(\gamma') &= ((R_+(\gamma) \cap M') \cup S'_+) \setminus \text{Int}(\gamma'), \\ R_-(\gamma') &= ((R_-(\gamma) \cap M') \cup S'_-) \setminus \text{Int}(\gamma'). \end{aligned}$$

Here S'_+ (resp. S'_-) is the component of $\partial N(S) \cap M'$ whose normal vector points out of (resp. into) M' .

Remark 2.8. In other words, the sutured manifold (M', γ') is constructed by splitting M along S , creating $R_+(\gamma')$ by adding S'_+ to what is left of $R_+(\gamma)$ and creating $R_-(\gamma')$ by adding S'_- to what is left of $R_-(\gamma)$. Finally, one creates the annuli of γ' by “thickening” $R_+(\gamma') \cap R_-(\gamma')$.

The following lemma indicates that Examples 2.5 and 2.6 are connected by a sutured manifold decomposition.

Lemma 2.9. *Suppose that R is a Seifert surface for a knot $K \subset Y$. Then*

$$Y_{2n}(K) \xrightarrow{\sim^R} Y(R) .$$

2.2. Sutured Floer homology. We can associate to a balanced sutured manifold a collection of abelian groups, called the sutured Floer homology groups [10]. These groups are the homology groups of a chain complex, which is defined by a sutured Heegaard diagram. Sutured Heegaard diagrams generalize Heegaard diagrams of closed 3-manifolds so that we can also describe sutured manifolds.

Definition 2.10. A *sutured Heegaard diagram* is a tuple (Σ, α, β) , where Σ is a compact oriented surface with boundary and $\alpha = \{\alpha_1, \dots, \alpha_m\}$ and $\beta = \{\beta_1, \dots, \beta_n\}$ are two sets of pairwise disjoint simple closed curves in $\text{Int}(\Sigma)$.

Every sutured Heegaard diagram (Σ, α, β) uniquely defines a sutured manifold (M, γ) using the following construction: Let M be the 3-manifold obtained from $\Sigma \times I$ by attaching 3-dimensional 2-handles along the curves $\alpha_i \times \{0\}$ and $\beta_j \times \{1\}$ for $i = 1, \dots, m$ and $j = 1, \dots, n$. The sutures are defined by taking $\gamma = \partial M \times I$ and $s(\gamma) = \partial M \times \{1/2\}$.

Definition 2.11. A sutured Heegaard diagram (Σ, α, β) is called *balanced* if $|\alpha| = |\beta|$ and the maps $\pi_0(\partial\Sigma) \rightarrow \pi_0(\Sigma \setminus \bigcup \alpha)$ and $\pi_0(\partial\Sigma) \rightarrow \pi_0(\Sigma \setminus \bigcup \beta)$ are surjective.

The following is [10, Proposition 2.14].

Proposition 2.12. *For every balanced sutured manifold (M, γ) there exists a balanced diagram defining it.*

In order to understand how *SFH* behaves under surface decompositions, it is necessary to understand these operations at the level of Heegaard diagrams. To this end, we have the following definition (Definition 4.3 of [11]).

Definition 2.13. A balanced diagram *adapted* to the decomposing surface R in (M, γ) is a quadruple

$$(\Sigma, \alpha, \beta, P),$$

satisfying the following conditions.

- (1) (Σ, α, β) is a balanced diagram of (M, γ) .
- (2) $P \subset \Sigma$ is a quasi-polygon (i.e., a closed subsurface of Σ whose boundary is a union of polygons) such that $P \cap \partial\Sigma$ is exactly the set of vertices of P .
- (3) There is a decomposition $\partial P = A \cup B$, where both A and B are unions of pairwise disjoint edges of P satisfying $\alpha \cap B = \emptyset$ and $\beta \cap A = \emptyset$ for every $\alpha \in \alpha$ and $\beta \in \beta$.
- (4) R is obtained, up to equivalence, by smoothing the corners of the surface $(P \times \{1/2\}) \cup (A \times [1/2, 1]) \cup (B \times [0, 1/2]) \subset (M, \gamma)$ (recall the construction following Definition 2.10).
- (5) The orientation of R is given by the orientation of $P \subset \Sigma$.

We will frequently refer to a diagram adapted to R as a *surface diagram*. A surface diagram allows us to represent decomposition along R in terms of Heegaard diagrams. To describe this process, let $(\Sigma, \alpha, \beta, P)$ be a surface diagram for R . To such a diagram, we can uniquely associate a six-tuple

$$D(P) = (\Sigma', \alpha', \beta', P_A, P_B, p).$$

Here, $(\Sigma', \alpha', \beta')$ is a balanced diagram, $p: \Sigma' \rightarrow \Sigma$ is a smooth map, and $P_A, P_B \subset \Sigma'$ are two closed subsurfaces (see Figure 2.1). We will refer to $D(P)$ as the *decomposed diagram*. $D(P)$ is constructed as follows.

We begin with Σ' . Let P_A and P_B be two disjoint copies of P , together with diffeomorphisms $p_A: P_A \rightarrow P$ and $p_B: P_B \rightarrow P$. Then

$$\Sigma' = P_A \bigsqcup_{p_A^{-1}(A) \leftrightarrow A} \overline{(\Sigma \setminus P)} \bigsqcup_{p_B^{-1}(B) \leftrightarrow B} P_B.$$

Thus, Σ' is obtained by removing P from Σ , and then gluing two copies of P to the closure of the remaining surface, one copy glued along its A edges and the other along its B edges.

The map $p: \Sigma' \rightarrow \Sigma$ agrees with p_A on P_A and p_B on P_B , and it maps $\Sigma' \setminus (P_A \cup P_B)$ to $\Sigma \setminus P$ using the obvious diffeomorphism.

Finally, let

$$\begin{aligned} \alpha' &= \{p^{-1}(\alpha) \setminus P_B : \alpha \in \alpha\}, \\ \beta' &= \{p^{-1}(\beta) \setminus P_A : \beta \in \beta\}. \end{aligned}$$

Thus p is $1:1$ over $\Sigma \setminus P$, is $2:1$ over P , and α curves are lifted to P_A and β curves to P_B . For the purposes of sutured Floer homology computations it is useful to note that, given a conformal structure on Σ , there is a unique conformal structure on Σ' making p into a conformal map. The following proposition indicates that the decomposed diagram produces a Heegaard diagram for the sutured manifold obtained by decomposing along R .

Proposition 2.14. ([11, Proposition 5.2]) *Let (M, γ) be a balanced sutured manifold and*

$$(M, \gamma) \rightsquigarrow^S (M', \gamma')$$

a surface decomposition. If $(\Sigma, \alpha, \beta, P)$ is a surface diagram adapted to S and if

$$D(P) = (\Sigma', \alpha', \beta', P_A, P_B, p)$$

is the decomposed diagram, then $(\Sigma', \alpha', \beta')$ is a balanced diagram defining (M', γ') .

2.2.1. The sutured Floer chain complex. We conclude this section by briefly recalling the definition of the sutured Floer chain complex, and describing the splitting of this complex along relative Spin^c structures.

Given a balanced sutured Heegaard diagram, (Σ, α, β) , for a balanced sutured manifold, (M, γ) , one can define a chain complex $(C(\Sigma, \alpha, \beta), \partial)$. As a $\mathbb{Z}/2\mathbb{Z}$ vector space, $C(\Sigma, \alpha, \beta)$ is generated by k -tuples $\mathbf{x} = x_1 \times \cdots \times x_k$ of intersection points, where $x_i \in \alpha_i \cap \beta_{\sigma(i)}$ (here, σ is a permutation in the symmetric group on k letters and $k = |\alpha| = |\beta|$ is the number of α curves). If $k = 0$, then despite having no curves we have a single generator (for the familiar reader, this is due to the fact that the 0-th symmetric product of Σ is a point, which coincides with the intersection of the two lagrangians).

The chain complex is equipped with a differential ∂ which counts points in moduli spaces of certain pseudo-holomorphic maps [26, 16]. To describe this, let us call the connected components of $\Sigma - \alpha - \beta$ *regions*, and denote them by $\mathcal{D}_1, \dots, \mathcal{D}_j$. Given two generators $\mathbf{x}, \mathbf{y} \in C(\Sigma, \alpha, \beta)$ consider a linear combination of regions

$$\phi = \sum_{i=1}^j n_i \cdot \mathcal{D}_i$$

which satisfies $\partial(\partial\phi|_\alpha) = \mathbf{y} - \mathbf{x}$, i.e., the oriented boundary of the α components of $\partial\phi$ consists of the k -tuples of intersection points which comprise $-\mathbf{x}$ and \mathbf{y} . If, furthermore, $\phi \cap \partial\Sigma = \emptyset$, we say that ϕ is a *domain* connecting \mathbf{x} to \mathbf{y} . Let us denote by $\pi_2(\mathbf{x}, \mathbf{y})$ the set of domains connecting \mathbf{x} to \mathbf{y} .

We define an endomorphism ∂ of $C(\Sigma, \alpha, \beta)$ by specifying it on generators:

$$\partial\mathbf{x} = \sum_{\mathbf{y} \in C(\Sigma, \alpha, \beta)} \sum_{\{\phi \in \pi_2(\mathbf{x}, \mathbf{y}) \mid \mu(\phi)=1\}} \#\widehat{\mathcal{M}}(\phi) \cdot \mathbf{y}.$$

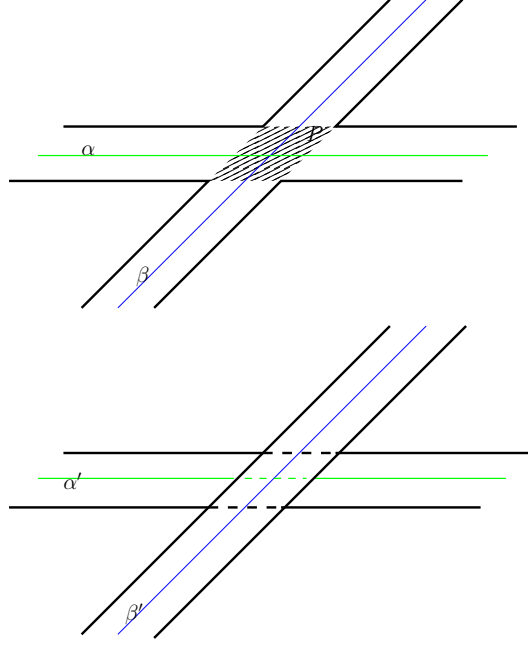


FIGURE 2.1. Balanced diagram before and after a surface decomposition

In the formula, $\#\widehat{\mathcal{M}}(\phi)$ denotes the number (modulo 2) of unparameterized pseudo-holomorphic maps of the unit disk $D^2 \subset \mathbb{C}$ into the k -fold symmetric product of Σ , satisfying boundary conditions specified by $(\alpha, \beta, \mathbf{x}, \mathbf{y})$ and whose homotopy class is determined by ϕ . The quantity $\mu(\phi)$ is the Maslov index of the domain, ϕ , and the condition $\mu(\phi) = 1$ is in place to ensure that the count can be performed (i.e., there exist only finitely many). We refer the reader to [10] for more details on the definition of ∂ , but do call to mind the following important property (see Lemma 3.2 of [26])

Lemma 2.15. *Let $\phi = \sum_{i=1}^j n_i \cdot \mathcal{D}_i$ be a domain. If $\#\widehat{\mathcal{M}}(\phi) \neq 0$, then $n_i \geq 0$ for all i .*

For the purposes of computation, it is also useful to know that ∂ can be reformulated in terms of counting holomorphic maps of surfaces with boundary (and with marked points on the boundary) into $\Sigma \times D^2$. This is made precise in [16].

The following is contained in Theorems 7.1 and 7.5 of [10]

Theorem 2.16. *Let (Σ, α, β) be a Heegaard diagram for the sutured manifold, (M, γ) , and let $(C(\Sigma, \alpha, \beta), \partial)$ be as above. Then $\partial^2 = 0$. The resulting homology groups, denoted $SFH(M, \gamma)$, depend only on the equivalence class of sutured manifold.*

The above theorem suppresses some extra structure which we now discuss; namely, the splitting of sutured Floer homology into subgroups indexed by the set of *relative* Spin^c structures on (M, γ) , which we denote $\underline{\text{Spin}}^c(M, \gamma)$. Indeed, to a generator $\mathbf{x} \in C(\Sigma, \alpha, \beta)$ one can associate a relative Spin^c structure, $\mathfrak{s}(\mathbf{x}) \in \underline{\text{Spin}}^c(M, \gamma)$, as follows.

First, pick a Morse function which determines the Heegaard diagram and whose gradient vector field points into M along $R_-(\gamma)$, points out of M along $R_+(\gamma)$, and which is the gradient of the height function

$s(\gamma) \times I \rightarrow I$ on γ . Next, modify the gradient field in a neighborhood of flowlines specified by $x_i \in \mathbf{x}$. This produces a non-vanishing vector field, v , with prescribed behavior on ∂M . The homology class of v (in the sense of Turaev [31]) specifies a relative Spin^c structure, which we denote by $\mathfrak{s}(\mathbf{x})$. The “relative” terminology arises since we require vector fields to have prescribed behavior on ∂M . See Section 4 of [10] for more details.

For our purposes, the most important aspect of $\text{Spin}^c(M, \gamma)$ is that it is an affine set for $H^2(M, \partial M; \mathbb{Z})$. This implies, in particular, that we can talk about the difference of two relative Spin^c structures, $\mathfrak{s}(\mathbf{x}) - \mathfrak{s}(\mathbf{y}) \in H^2(M, \partial M; \mathbb{Z})$. Given two generators, \mathbf{x}, \mathbf{y} , we can concretely determine $\mathfrak{s}(\mathbf{x}) - \mathfrak{s}(\mathbf{y})$ as follows. First pick a collection of k oriented sub-arcs of the α curves, $\gamma_\alpha \subset \alpha$, which connect the intersection points x_i to y_i . Similarly, pick a collection of k oriented sub-arcs of the β curves, $\gamma_\beta \subset \beta$, which connect the intersection points y_i to $x_{\sigma(i)}$, for some permutation σ . The sum, $\gamma_{\mathbf{x}, \mathbf{y}} = \gamma_\alpha + \gamma_\beta$, is a collection of oriented closed curves in $\Sigma \subset M$ whose homology class we denote by $\epsilon(\mathbf{x}, \mathbf{y}) \in H_1(M; \mathbb{Z})$. The following lemma is quite useful.

Lemma 2.17. (Lemma 4.7 of [10]) *Let $\mathbf{x}, \mathbf{y} \in C(\Sigma, \alpha, \beta)$ be generators. Then*

$$\mathfrak{s}(\mathbf{x}) - \mathfrak{s}(\mathbf{y}) = \text{PD}[\epsilon(\mathbf{x}, \mathbf{y})] \in H^2(M, \partial M; \mathbb{Z}),$$

where $\text{PD}[\epsilon(\mathbf{x}, \mathbf{y})]$ denotes the Poincaré dual of $\epsilon(\mathbf{x}, \mathbf{y})$.

The lemma makes clear the claim from the introduction; namely, that $(C(\Sigma, \alpha, \beta), \partial)$ splits as a direct sum of complexes which are indexed by relative Spin^c structures. To see this, first observe that $(C(\Sigma, \alpha, \beta), \partial)$ splits into subcomplexes corresponding to the equivalence classes of the relation

$$\mathbf{x} \sim \mathbf{y} \iff \pi_2(\mathbf{x}, \mathbf{y}) \neq \emptyset.$$

Next, note that if $\phi \in \pi_2(\mathbf{x}, \mathbf{y})$ then $\epsilon(\mathbf{x}, \mathbf{y}) = [\partial\phi] = 0 \in H_1(M; \mathbb{Z})$. Thus, if \mathbf{x} and \mathbf{y} are in the same subcomplex, they represent the same Spin^c structure. Conversely, if \mathbf{x} and \mathbf{y} represent the same Spin^c structure, then $\epsilon(\mathbf{x}, \mathbf{y}) = 0 \in H_1(M; \mathbb{Z})$. In light of the isomorphism,

$$H_1(M; \mathbb{Z}) \cong \frac{H_1(\Sigma; \mathbb{Z})}{\text{Span}_i([\alpha_i] + [\beta_i])},$$

this implies that after possibly adding some copies of the α and β curves to $\gamma_{\mathbf{x}, \mathbf{y}}$, we obtain a collection of curves which are null-homologous in Σ . A null-homology is an element $\phi \in \pi_2(\mathbf{x}, \mathbf{y})$.

We have the following refinement of the theorem stated above:

Theorem 2.18. *Let (M, γ) be a sutured manifold. Then*

$$SFH(M, \gamma) = \bigoplus_{\mathfrak{s} \in \text{Spin}^c(M, \gamma)} SFH(M, \gamma, \mathfrak{s})$$

The homology group $SFH(M, \gamma, \mathfrak{s})$, depends only on the equivalence class of the sutured manifold and the relative Spin^c structure \mathfrak{s} .

One of the most important aspects of sutured Floer homology is its behavior under surface decompositions, which we now describe. We will need a definition. As above, suppose we have a decomposition

$$(M, \gamma) \xrightarrow{S} (M', \gamma').$$

Let $(\Sigma, \alpha, \beta, P)$ be a surface diagram for S . Denote by $\mathcal{O}_P \subset \mathbb{T}_\alpha \cap \mathbb{T}_\beta$ the subset of generators, none of whose intersection points $x_i \in \mathbf{x}$ are contained in the quasipolygon, $P \subset \Sigma$. Call such generators *outer generators*. The *outer complex* $C(\mathcal{O}_P) \subset C(\Sigma, \alpha, \beta)$ is the subcomplex generated by \mathcal{O}_P . Finally, let $C(\Sigma', \alpha', \beta')$ be the chain complex associated to the decomposed diagram. The main result of [11] is the following.

Theorem 2.19. *The outer complex, $C(\mathcal{O}_P) \subset C(\Sigma, \alpha, \beta)$, forms a subcomplex. Moreover, the homology of this subcomplex is isomorphic to the homology of $C(\Sigma', \alpha', \beta')$. In particular,*

$$SFH(M', \gamma') := H_*(C(\Sigma', \alpha', \beta')) \cong H_*(C(\mathcal{O}_P)) \leq SFH(M, \gamma),$$

where \leq means “direct summand”.

Proof. (sketch) To see that $C(\mathcal{O}_P)$ forms a subcomplex, consider a generator $\mathbf{y} \in (\mathbb{T}_\alpha \cap \mathbb{T}_\beta) \setminus \mathcal{O}_P$. We will show that $\pi_2(\mathbf{x}, \mathbf{y}) = \emptyset$ for every $\mathbf{x} \in \mathcal{O}_P$. This implies that $\mathbf{y} \notin \partial\mathbf{x}$ for every $\mathbf{x} \in \mathcal{O}_P$, and repeating with each $\mathbf{y} \in (\mathbb{T}_\alpha \cap \mathbb{T}_\beta) \setminus \mathcal{O}_P$ we see that $\partial C(\mathcal{O}_P) \subset C(\mathcal{O}_P)$, i.e., $C(\mathcal{O}_P)$ is a subcomplex.

To see that $\pi_2(\mathbf{x}, \mathbf{y}) = \emptyset$ for \mathbf{x}, \mathbf{y} as above, consider the collection of curves $\gamma_{\mathbf{x}, \mathbf{y}} = \gamma_\alpha + \gamma_\beta$ connecting \mathbf{x} to \mathbf{y} . Pushing γ_α into the α handlebody and γ_β into the β handlebody, we obtain an oriented collection of curves, $\tilde{\gamma}_{\mathbf{x}, \mathbf{y}} \subset M$. Note that since γ_α is oriented from x_i to y_i , each intersection of $\tilde{\gamma}_{\mathbf{x}, \mathbf{y}}$ with the quasipolygon P is positive. Since the only intersections $\tilde{\gamma}_{\mathbf{x}, \mathbf{y}} \cap S$ occur in P , this shows that $\#_{alg}(\tilde{\gamma}_{\mathbf{x}, \mathbf{y}} \cap S) > 0$. In particular $\epsilon(\mathbf{x}, \mathbf{y}) = [\tilde{\gamma}_{\mathbf{x}, \mathbf{y}}] \neq 0$, showing that $\pi_2(\mathbf{x}, \mathbf{y}) = \emptyset$.

Now it is immediate from the construction of the decomposed diagram that generators of $C(\Sigma', \alpha', \beta')$ are in bijection with \mathcal{O}_P . Indeed, since α and β arcs in P lift to P_A and P_B in the decomposed diagram, respectively, no intersection point $x_i \in P \subset \Sigma$ will lift to an intersection point in Σ' (since $P_A \cap P_B = \emptyset$). Hence any generator \mathbf{x} containing $x_i \in P$ will not lift to a generator for $C(\Sigma', \alpha', \beta')$. On the other hand, the decomposed diagram is identical to the surface diagram (before decomposition) outside of P . Thus any outer generator lifts to a generator in $C(\Sigma', \alpha', \beta')$.

The most challenging part of the the proof arises when showing that the differential on $C(\Sigma', \alpha', \beta')$ is identical to the differential on $C(\mathcal{O}_P)$ which it inherits as a subcomplex of $C(\Sigma, \alpha, \beta)$. To prove this, [11] adapts the algorithm of [28] for computing Heegaard Floer homology to the context of sutured Floer homology. By making the surface diagram “nice”, the count of pseudo-holomorphic curves for each domain $\phi \in \pi_2(\mathbf{x}, \mathbf{y})$ with $\mu(\phi) = 1$ can be done explicitly using the Riemann mapping theorem, together with the fact that pseudo-holomorphic submanifolds of symplectic manifolds intersect positively. Moreover, for a nice enough surface diagram, the decomposed diagram will also be nice and one can explicitly identify the differentials for the respective complexes. See [11] for more details. \square

As a corollary, one obtains the theorem mentioned in the introduction.

Theorem 2.20. *Let R be a Seifert surface for a knot $K \subset S^3$. Then*

$$SFH(S^3(R)) \cong \widehat{HFK}(K, g(R)),$$

where the right hand side is the knot Floer homology group of K supported in Alexander grading $g(R)$ [24].

Proof. (sketch) By Lemma 2.9 if we decompose $S^3_2(K)$ along R we get $S^3(R)$. Let $(\Sigma, \alpha, \beta, P)$ be a surface diagram adapted to R . The Alexander grading of a generator $\mathbf{x} \in C(\Sigma, \alpha, \beta) \cong \widehat{CFK}(K)$ can be defined as

$$\frac{1}{2} \langle c_1(\mathfrak{s}(\mathbf{x})), [R, \partial R] \rangle,$$

where $c_1(\mathfrak{s}(\mathbf{x})) \in H^2(S^3 \setminus N(K), \partial; \mathbb{Z})$ is the relative Chern class of a relative Spin^c structure associated to \mathbf{x} and $[R, \partial R] \in H_2(S^3 \setminus N(K), \partial; \mathbb{Z})$ is the homology class of the surface. This evaluation, in turn, can be computed as

$$\chi(R) - 1 + \#\{x_i \in \mathbf{x} \mid x_i \in P\},$$

where P is the quasi-polygon representing R (see the proof of Theorem 5.1 of [24] for motivation of this formula and [11] for precise details). Together with Theorem 2.19, this shows that

$$SFH(S^3(R)) \cong \widehat{HFK}(K, -g(R)).$$

However, $\widehat{HFK}(K, g(R)) \cong \widehat{HFK}(K, -g(R))$ by Proposition 3.10 of [24]. \square

3. CONSTRUCTING HEEGAARD DIAGRAMS ADAPTED TO A SEIFERT SURFACE

Given a Seifert surface R for a knot $K \subset Y$, we wish to compute the sutured Floer homology groups, $SFH(Y(R))$. Since these groups are the homology of a chain complex associated to a balanced sutured Heegaard diagram for $Y(R)$, it is necessary to produce such a diagram. To do this, recall that $Y(R)$ is obtained from the knot complement $Y_{2n}(K)$ by decomposition along R . According to Section 2, it suffices to produce a balanced diagram for $Y_{2n}(K)$ which is adapted to R . From there it is simple to obtain the decomposed diagram. This section will be dedicated to producing surface diagrams and clarifying the decomposed diagram which, by Proposition 2.14, will necessarily be adapted to $Y(R)$. Throughout we assume the genus of R to be g .

A surface diagram for R is, by definition, a Heegaard diagram for the sutured manifold associated to the knot complement which contains R as a quasi-polygon. Building this diagram requires two main steps:

- (1) Construct a Heegaard diagram (Σ, α, β) for the closed three-manifold, Y , which contains R as proper subsurface, $R \subset \Sigma$.
- (2) Remove disks from Σ along ∂R , and modify the diagram by a sequence of isotopies and/or stabilizations to ensure that the diagram specifies $Y_{2n}(K)$ and is adapted to R .

For any given Seifert surface, there are many ways to perform each step so we remain intentionally vague for the moment. The next two subsections discuss each step in detail. Indeed, for both steps we treat the case of a Seifert surface presented in an arbitrary manner. This has the advantage of being completely general and should thus be useful in a variety of situations.

For the sake of clarity, the third subsection presents explicit diagrams for the case of knots in S^3 with Seifert surfaces presented in a particularly appealing form. The presentation is analogous to a knot projection, and the surface diagrams which we produce can be viewed as the analogue of the diagrams used by Ozsváth and Szabó in [21] which connect the knot Floer homology chain complexes to Kauffman states.

3.1. Constructing a diagram for Y containing R . Let $R \subset Y$ be an embedded surface with non-empty boundary. We now describe the construction of a Heegaard diagram (Σ, α, β) which contains R as an embedded, proper subsurface of Σ . Similar diagrams have been useful in other contexts [24, 22, 19]

Begin with R . Now thicken to obtain $R \times I$. This is a handlebody of genus $2g$. We can represent a basis for $H_1(R, \partial R; \mathbb{Z})$ by $2g$ pairwise disjoint properly embedded arcs, γ_i , $i = 1, \dots, 2g$. Observe that $\gamma_i \times I$ is a properly embedded disk in the handlebody $R \times I$. Let $\beta_i = \partial(\gamma_i \times I)$. Note that $\partial(R \times I)$ consists of two copies of R , glued along ∂R . Thus $\partial(R \times I)$ clearly contains R as an embedded proper subsurface.

Now $Y \setminus R \times I$ is not necessarily a handlebody (indeed, it will be a handlebody precisely when R is a so-called *free* Seifert surface). By adding a collection of three-dimensional 1-handles, $\{h_i\}_{i=1}^k$ to $R \times I$ we can ensure that

$$H_\alpha = Y \setminus (R \times I \cup h_1 \cup \dots \cup h_k)$$

is a handlebody (of genus $2g + k$). Without loss of generality, we may assume that the feet of the 1-handles lie on $R \times \{0\}$, so that $R = R \times \{1\} \subset \partial H_\alpha$ is still embedded. Let β_i denote the belt spheres of the 1-handles, $i = 2g + 1, \dots, 2g + k$.

Finally, pick a collection $\{\alpha_i\}_{i=1}^{2g+k}$ of linearly independent curves on $\Sigma_{2g+k} = \partial H_\alpha$ which bound disks in H_α . Then

$$(\Sigma_{2g+k}, \{\alpha_1, \dots, \alpha_{2g+k}\}, \{\beta_1, \dots, \beta_{2g+k}\})$$

is the desired Heegaard diagram.

Remark 3.1. Note that, by construction, the Heegaard diagram

$$(\Sigma_{2g+k}, \{\alpha_1, \dots, \alpha_{2g+k}\}, \{\beta_{2g+1}, \dots, \beta_{2g+k}\})$$

(i.e., the Heegaard diagram of the lemma without the first $2g$ β curves) specifies $Y \setminus R \times I$.

3.2. Turning the diagram into a surface diagram. Having produced a Heegaard diagram for Y containing R , we now describe how to turn this into a surface diagram for R .

Begin with the Heegaard diagram of Subsection 3.1. The desired result is achieved through the following algorithm (see Figure 3.1 for a depiction of the algorithm):

- (1) Pick two points $\{z, w\} \subset K = \partial R$. The points divide K into two arcs, which we label by A and B . Remove disc neighborhoods $\{D(z), D(w)\} \subset \Sigma$ of the two points and call the resulting surface-with-boundary Σ .
 If $A \cap \beta_i = \emptyset$, $B \cap \alpha_i = \emptyset$ for all i then we are done. If not, proceed to Step 2.
- (2) Without loss of generality, assume $p \in A \cap \beta_i$ (if $p \in B \cap \alpha_i$, the same process applies with the roles of A and B , α and β reversed). Remove p by one of the following operations.
 - **Isotopy:** Starting from p , perform a finger move of β_i along the A arc until a boundary component of Σ is reached. If other β curves are encountered, perform the finger move to these curves as well to ensure that no intersections among β curves are created. Handleslide β_i , along with any other curves picked up by the isotopy, over the boundary component of Σ .
 - **Stabilization:** Choose a sub-arc, γ , of the A arc containing p , which satisfies $\gamma \cap \alpha_i = \emptyset$ for all i . Subdivide K so that γ is labeled B and the two arcs adjacent to γ are labeled A . Let $D(\gamma)$ be a neighborhood of γ . Adjoin $\partial(D(\gamma))$ to the collection of α curves. Similarly, pick one of the two A arcs adjacent to γ , and adjoin the boundary of its neighborhood to the β curves. Finally, remove neighborhoods of the endpoints of γ from Σ .
- (3) If $A \cap \beta_i = \emptyset$, $B \cap \alpha_i = \emptyset$ for all i then we are done. If not, repeat Step 2.

Proposition 3.2. *The above algorithm terminates at a surface diagram adapted to R .*

Proof. As there are only a finite number of points in the initial set $\{A \cap \beta_i, B \cap \alpha_i\}$, it is clear that the above algorithm terminates. To see that we have produced a surface diagram, first observe that the algorithm can be reinterpreted as an algorithm to convert the original diagram into a multi-pointed Heegaard diagram for $K \subset Y$. Indeed, instead of removing neighborhoods of $\{z, w\}$ and the endpoints of γ in Steps 1 and 2, respectively, we could simply keep track of these points as pairs $\{z_i, w_i\}$ (and labeling so that z 's are always the initial point of some A arc, oriented by the orientation of K). The resulting multi-pointed Heegaard diagram is then adapted to K , in the sense of Definition 2.1 of [18]. Generalizing Example 2.4 and Proposition 9.2 of [10] to the case of multi-pointed diagrams shows that removing neighborhoods of the basepoints produces a balanced diagram adapted $Y_{2n}(K)^2$.

Finally, observe that since the original diagram contained R as a proper subsurface, the terminal diagram contains R as a quasi-polygon of the desired form. Indeed, the A and B edges of the quasi-polygon are the A and B arcs produced by the algorithm. Strictly speaking, we must make a local modification to these arcs as specified by Figure 3.2 to ensure that ∂R is of the appropriate form. □

²Note that n is the number of stabilizations performed in the algorithm +1.

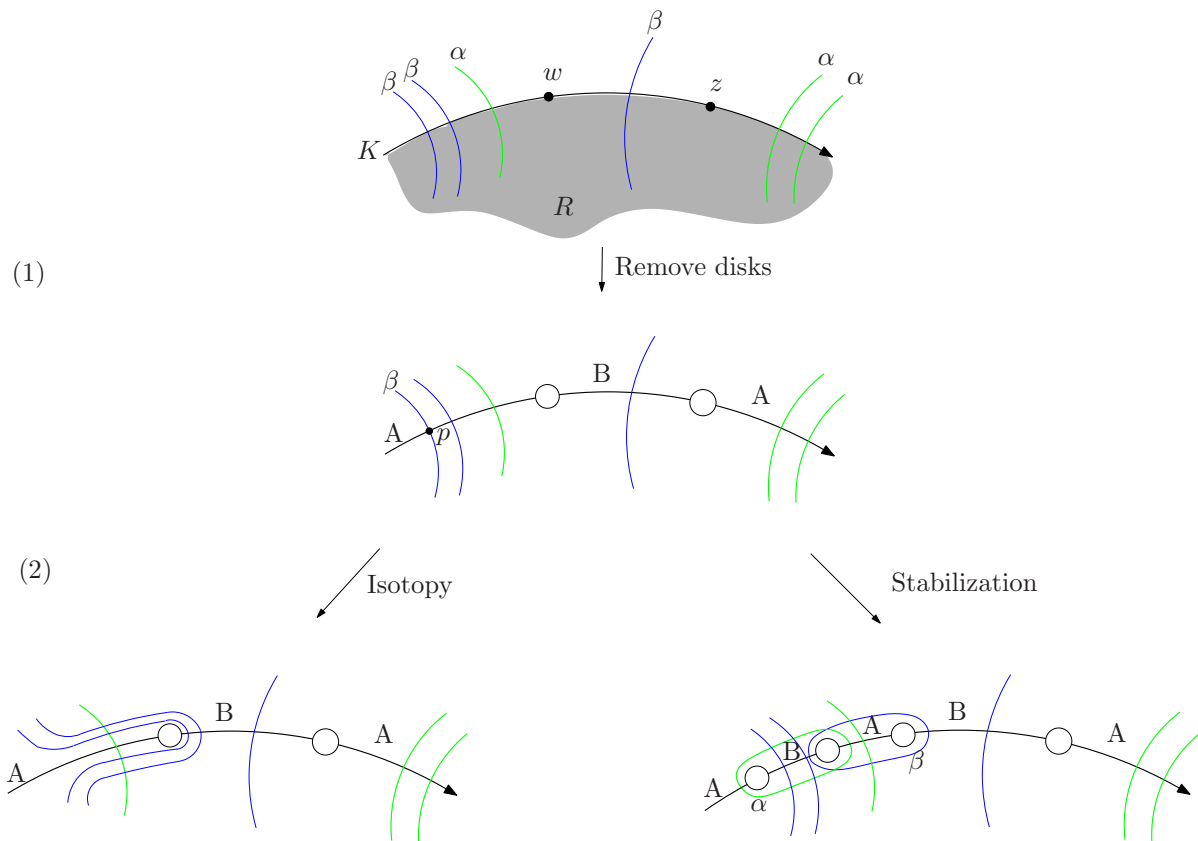


FIGURE 3.1.

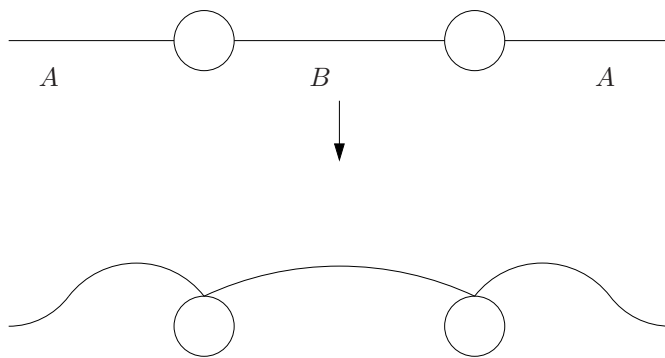


FIGURE 3.2.

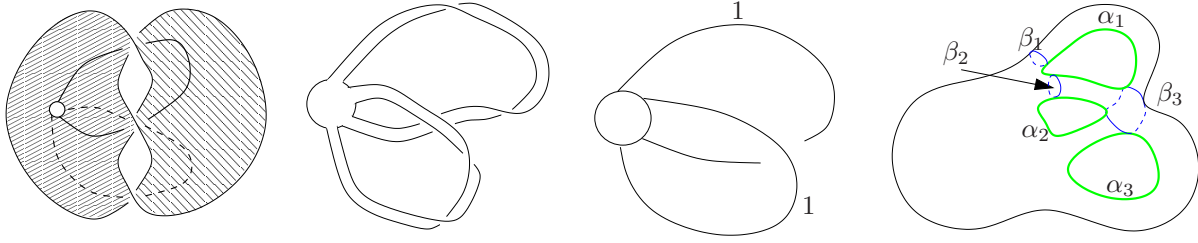


FIGURE 3.3. Starting from a Seifert surface for the trefoil, we first retract to a neighborhood of a one skeleton possessing a single 0-cell. We then encode this surface with a planar diagram, where 1's indicate that the corresponding bands have a full right-handed twist. The third shows the handlebody which results from thickening the diagram. The thick green curves are α -curves specifying the complementary handlebody. Each band contributes a thin blue β curve. The final β curve comes from the crossing in the diagram, according to Figure 3.4 below.



FIGURE 3.4.

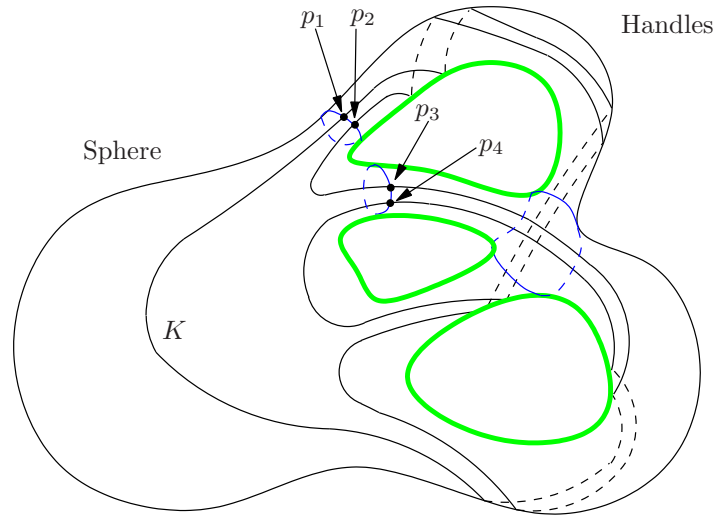


FIGURE 3.5.

3.3. Explicit Heegaard diagrams for Seifert surfaces in S^3 . We now describe an explicit diagram adapted to a Seifert surface in S^3 .

To begin, we isotope R so that it consists of a disc with $2g$ bands attached to it. One way to do this is to note that since R is a surface with one boundary component, it is homotopy equivalent to a CW complex with one 0-cell and $2g$ 1-cells. Represent the 0-cell by a disk neighborhood, D , of an interior point. Represent the 1-cells by $2g$ disjoint arcs on R , each of whose endpoints lie in ∂D . Now let F be a regular neighborhood of D and the $2g$ arcs. Then R deformation retracts onto F and ∂R stays an embedded circle in S throughout. This induces an isotopy which takes (R, K) to $(F, \partial F)$. Indeed, if the surface R is presented in some nice fashion then this gives an algorithm to get such a pair $(F, \partial F)$. An example of this construction is shown in Figure 3.3 for the minimal genus Seifert surface of the trefoil.

Assuming, then, that R is represented as above, proceed by contracting each band of R to an arc. We may assume that the resulting disk with $2g$ arcs lies in a subset homeomorphic to \mathbb{R}^3 and, moreover, that there exists a plane $\mathbb{R}^2 \subset \mathbb{R}^3$ onto which projection yields a planar diagram satisfying:

- The disc (0-handle) of R is embedded in \mathbb{R}^2 and no arc is projected to its interior.
- The arcs have only finitely many transverse double points.

Keeping track of the crossing information at the double points, together with the framing of the band corresponding to each arc³, we obtain a planar diagram from which we can recover the surface, up to isotopy. Let k be the number of double points (crossings) in this planar diagram.

Proceed by thickening the diagram in \mathbb{R}^2 to obtain a handlebody, H_β , in \mathbb{R}^3 . The genus of H_β is $2g + k$, and we let $\Sigma = \partial H_\beta$ denote its boundary. Intersecting Σ with the original plane results in $(2g + k + 1)$ circles. Choose any $(2g + k)$ of these to be the α circles. Clearly, $(\Sigma, \alpha_1, \dots, \alpha_{2g+k})$ represents the complement of H_β .

Corresponding to each of the $2g$ arcs we obtain a β circle. This circle is the boundary of a disk which intersects the arc in a point close to the disc, D . Label these circles, β_i , $i = 1, \dots, 2g$. Finally, to each crossing in the planar diagram we add a β circle according to the convention of Figure 3.4. These circles are labeled $\beta_{2g+1}, \dots, \beta_{2g+k}$.

The resulting diagram

$$(\Sigma, \{\alpha_1, \dots, \alpha_{2g+k}\}, \{\beta_1, \dots, \beta_{2g+k}\})$$

represents S^3 and contains R by construction. An example of such a Heegaard diagram for the case of the trefoil is shown in Figure 3.3.

Next, we remove $8g$ discs from the Heegaard diagram while simultaneously adding $4g - 1$ pairs of α and β circles to adapt the diagram to R .

To describe this, first observe that the Heegaard surface can be divided into two parts; the *handles* and the (*punctured*) *sphere*. The handles arise from the boundary of a regular neighborhood of the arcs in the planar diagram, while the sphere comes from the boundary of a regular neighborhood of the disc D . Next, note that $K = \partial R$ is naturally embedded in Σ in such a way that it does not intersect the circles $\beta_{2g+1}, \dots, \beta_{2g+k}$, and intersects each of the other β circles exactly twice. See Figure 3.5

Up to isotopy in Σ , we can assume that K consists of two parallel strands in each handle. We can further assume that K lies mostly in the top part of Σ (namely, the part of Σ lying above the plane where the diagram of R was embedded). It passes to the bottom of Σ only in the handles to account for the framing and crossing information of the bands. For each of the $4g$ intersection points $\{p_{2i-1}, p_{2i}\} \in K \cap \beta_i$, $i = 1, \dots, 2g$, we remove two small discs from Σ next to p , one on either side of β_i . We denote the new surface-with-boundary by Σ' . Removing the discs separates K into $8g$ arcs, $\{A_j, B_j\}$, $j = 1, \dots, 4g$, with $p_j \in B_j$. For each $j \neq 4g$, we add a curve, α_{2g+k+j} , which encircles B_j together with the boundary components of Σ created

³Each band, b , comes with a framing which is $\#\{\text{full right-handed twists of } b\} - \#\{\text{full left-handed twists of } b\}$.

by removing the discs near the endpoints of B_j . Similarly, for each $j \neq 4g$ we add a curve, β_{2g+k+j} , which encircles A_j and the boundary components of Σ created by removing the discs near the endpoints of A_j .

Since Σ contained R before the discs were removed, it is straightforward to construct a quasi-polygon, $P \subset \Sigma'$, which satisfies the requirements of Definition 2.13. Indeed, the A and B edges of P are isotopic to the A and B arcs of the previous paragraph, as in Figure 3.2. We have arrived at a surface diagram for R :

$$(\Sigma', \{\alpha_1, \dots, \alpha_{6g+k-1}\}, \{\beta_1, \dots, \beta_{6g+k-1}\}, P)$$

See Figure 3.6 for the diagram adapted to the Seifert surface of the trefoil.

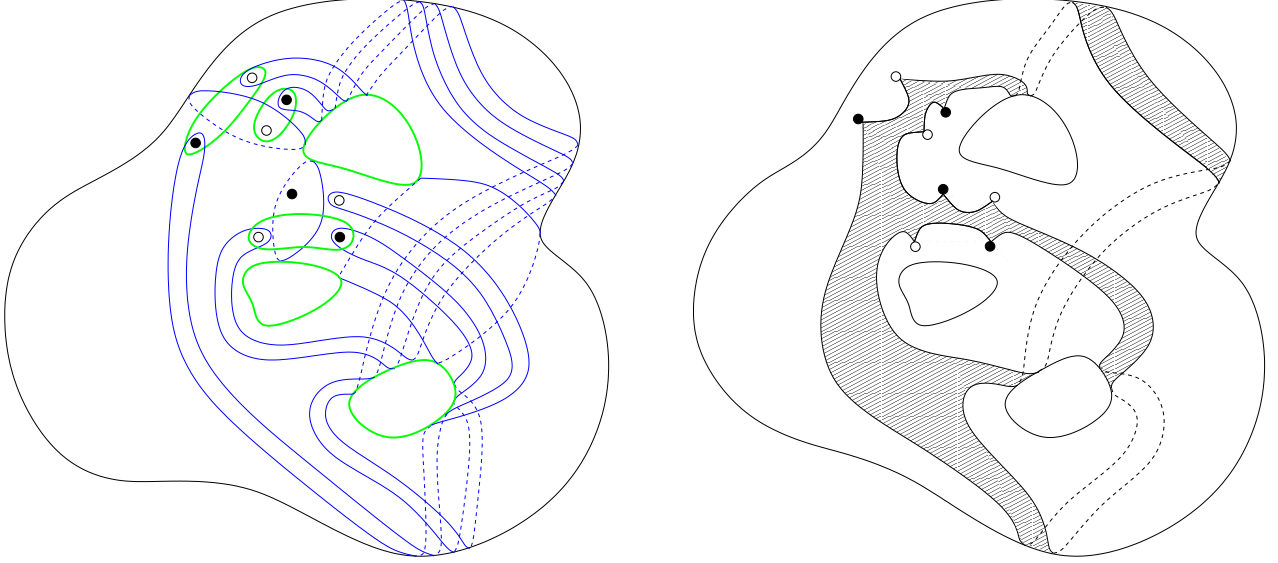


FIGURE 3.6. The Heegaard diagram

It is now easy to obtain a balanced diagram for the sutured manifold complementary to R : Delete the interior of P from the Heegaard diagram and take two copies of the subsurface. Delete all the α arcs in one of the copies and identify its B -arcs with the corresponding B -arcs in the Heegaard diagram. Similarly, delete all the β arcs in the other copy, and identify all its A -arcs with the corresponding A -arcs in the Heegaard diagram. The process is shown locally in the first part of Figure 3.7. The resulting balanced diagram represents $S^3(R)$. The Heegaard surface has genus $(7g + k - 1)$ and 1 boundary component, and has $(6g + k - 1)$ α circles and β circles each. The final sutured diagram for the trefoil example is shown in Figure 3.7.

Remark 3.3. The diagram above is a special case of the general construction discussed in the previous two subsections. The procedure by which we handled the crossing regions of the planar diagram associated to R is equivalent to adding 1-handles to $R \times I$ to make the complement into a handlebody. See Figure 3.8. Removing discs and adding α/β pairs is simply a specific implementation of the algorithm from Subsection 3.2. Indeed, the diagram of this subsection can be seen as extremal: at every step in the algorithm we used a stabilization. The other extremal case, where we use only isotopies, will be implemented in Section 4 to calculate the sutured Floer homology for the Seifert surfaces of 8_3 .

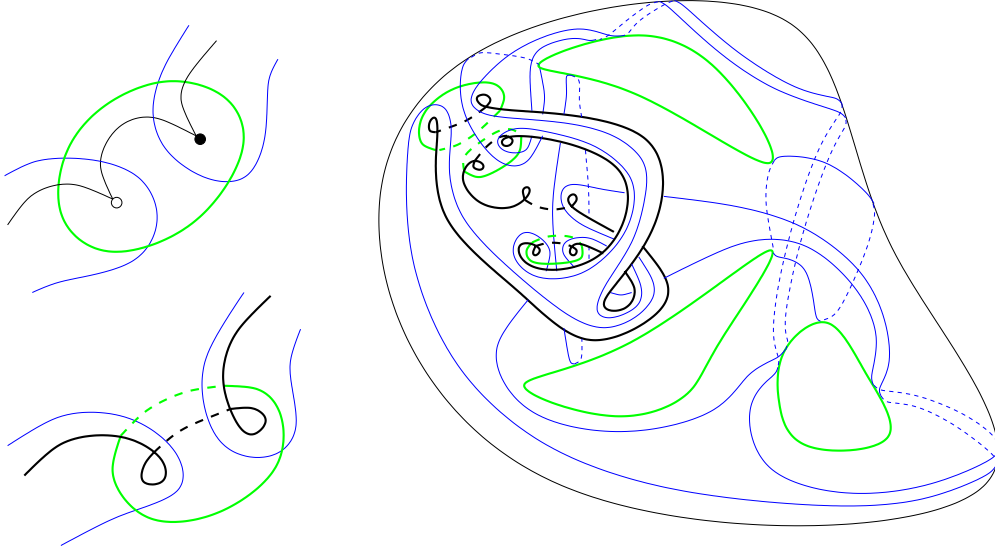


FIGURE 3.7. The sutured diagram

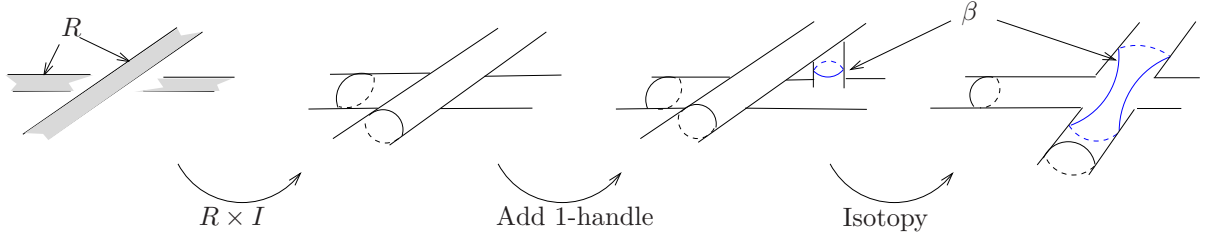


FIGURE 3.8.

Remark 3.4. The diagram above is usually not the minimal genus possible. Picking a different set of 1-handles to add to $R \times I$ will frequently lower the genus of the Heegaard diagram significantly. The minimal number of 1-handles necessary to add to an embedded handlebody, H_g , so that the complement is a handlebody is often referred to as the *tunnel number* of H_g .

While we do not use this diagram for the computation in the next section, it may be of future use to note that the combinatorics of the diagram enable one to calculate $SFH(S^3(R))$ without decomposing the diagram. More precisely, recall from the discussion surrounding Theorem 2.19 that the generators of the chain complex associated to the decomposed diagram are in bijection with the outer generators $C(\mathcal{O}_P)$ on the surface diagram. Indeed, Theorem 2.19 shows that the outer generators form a subcomplex of $SFH(S^3_{2n}(K))$ whose homology is isomorphic to $SFH(S^3(R))$. However, it is not clear that the obvious bijection between generators of $C(\mathcal{O}_P)$ and $SFH(S^3(R))$ induces the isomorphism on homology. The differentials on these two complexes could be quite different, as their definition is in terms of quite different Heegaard diagrams. It is only after altering the surface diagram severely to make it “nice” that an identification between the differentials is established. In light of this, it is nice to know that we can compute the homology of $SFH(S^3(R))$,

as a relatively $H_1(S^3 \setminus R)$ graded group, without decomposing the surface diagram. Indeed we have the following proposition

Proposition 3.5. *Let $\mathcal{H} = (\Sigma, \alpha, \beta, P)$ be the explicit surface diagram for a Seifert surface $R \subset S^3$ described above, and let $\mathcal{H}' = (\Sigma', \alpha', \beta')$ be the decomposed diagram. Denote the associated chain complexes by $(C(\mathcal{H}), \partial)$ and $(C(\mathcal{H}'), \partial')$. Then the differential on the subcomplex $C(\mathcal{O}_P) \subset C(\mathcal{H})$ generated by outer intersection points is equal to that on $C(\mathcal{H}')$, under the obvious isomorphism of chain groups induced by the bijection of generators. In particular, the relative Spin^c grading on $SFH(S^3(R))$ can be computed by considering the difference $\epsilon(\mathbf{x}, \mathbf{y})$ of two generators $\mathbf{x}, \mathbf{y} \in C(\mathcal{O}_P)$ as a 1-cycle in $H_1(S^3 \setminus R)$*

Remark 3.6. For more details on how to regard the difference $\epsilon(\mathbf{x}, \mathbf{y})$ of outer generators as an element in $H_1(S^3 \setminus R)$, see Subsection 4.3.2 below.

Proof. Let $\mathbf{x}, \mathbf{y} \in C(\mathcal{O}_P) \subset C(\mathcal{H})$ denote outer generators; that is, generators whose intersection points lie outside the quasi-polygon, P , representing R . Let $\mathbf{x}', \mathbf{y}' \in C(\mathcal{H}')$ denote the corresponding generators for the decomposed diagram. It suffices to show that

$$(1) \quad \mathbf{y} \in \partial \mathbf{x} \text{ if and only if } \mathbf{y}' \in \partial' \mathbf{x}'$$

(recall that we are working with $\mathbb{Z}/2\mathbb{Z}$ coefficients). Let $\phi \in \pi_2(\mathbf{x}, \mathbf{y})$ be a domain connecting the outer generators. Proving (1) will be accomplished by showing that $\widehat{\mathcal{M}}(\phi) \neq \emptyset$ implies $\phi \cap \{B\text{-arcs}\} = \emptyset$. In other words, the domains which contribute to ∂ do not intersect the B -arcs on the quasipolygon. To see why this implies (1), note that any ϕ satisfying $\phi \cap \{B\text{-arcs}\} = \emptyset$ can be thought of as $\phi' \in \pi_2(\mathbf{x}', \mathbf{y}')$, actually such domains are in one to one correspondence with domains on the decomposed diagram that support holomorphic representatives. Indeed, if ϕ' is a domain connecting \mathbf{x}' and \mathbf{y}' that has a holomorphic representative, then projecting this holomorphic map to Σ we see that $\phi = p(\phi')$ also has a holomorphic representative, thus $\phi \cap \{B\text{-arcs}\} = \emptyset$. Furthermore, for such domains, an almost complex structure on $\Sigma \times D^2$ achieving transversality for $\mathcal{M}(\phi)$ can be extended to an almost complex structure (under the embedding of $\Sigma \setminus B \subset \Sigma'$ away from the sutures) on $\Sigma' \times D^2$ which achieves transversality for $\mathcal{M}(\phi')$ (here we are thinking in terms of the cylindrical version of Floer homology [16]). In this way we see that if $\phi \cap \{B\text{-arcs}\} = \emptyset$, then $\widehat{\mathcal{M}}(\phi) \neq \emptyset$ if and only if $\widehat{\mathcal{M}}(\phi') \neq \emptyset$. Examining each ϕ , we obtain (1).

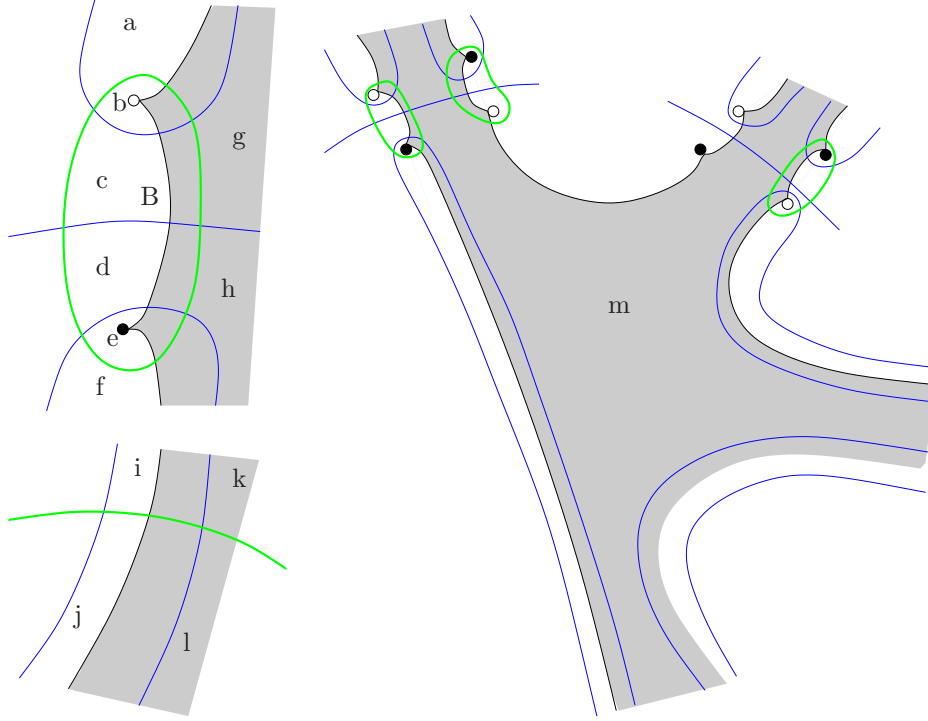
Thus we must only show that $\widehat{\mathcal{M}}(\phi) \neq \emptyset$ implies $\phi \cap \{B\text{-arcs}\} = \emptyset$. By contradiction, suppose that $\widehat{\mathcal{M}}(\phi) \neq \emptyset$ and $\phi \cap \{B\text{-arcs}\} \neq \emptyset$ for some domain ϕ . In Figure 3.9, we have marked various components of $\mathcal{H} \setminus (\alpha \cup \beta)$. The quasipolygon P is shaded. As usual, the thick green circles are α circles, and the thin blue circles are β circles. Let n_p be the multiplicity of ϕ in a region marked p . Recall from Lemma 2.15 that if $\widehat{\mathcal{M}}(\phi) \neq \emptyset$, then $n_p \geq 0$ for all $p \in \Sigma$.

Our first observation deals with the parts of the diagram that appear locally like the lower left part of the figure. We claim that for $\mathbf{x}, \mathbf{y} \in \mathcal{O}_P$, all domains satisfy $n_k - n_i = n_l - n_j$. This follows from the fact that $\mathbf{x}, \mathbf{y} \in \mathcal{O}_P$ implies there are no points of $\mathbf{x}, \mathbf{y} \in P$, and hence there are no corner points of ϕ contained in P .

Next we deal with the arcs in ϕ which hit the B arc shown in the first part of that figure. Label the regions in the handle part of \mathcal{H} by a, b, c and g and let the regions in the sphere part of \mathcal{H} be d, e, f and h . There are two cases.

- $n_d \neq 0$. Since $n_e = 0$ (e contains a suture) and \mathbf{x} and \mathbf{y} contain no points in P , $n_h - n_f = n_d - n_e > 0$. Thus $n_h > 0$, and since h is in the spherical part of \mathcal{H} , the region marked h is the same region as the disk region of R , marked m in the third part of Figure 3.9. But the disk part contains a suture, leading to a contradiction.

- $n_c \neq 0$. Again, since $n_b = 0$, a similar argument shows that $n_g - n_a > 0$. Proceed by examining the multiplicities of ϕ in the regions of the handle part of \mathcal{H} which border the β curve that separated a from g . Of course there may be α curves encountered on the way, as shown in the lower left part of Figure 3.9. However, our first observation above shows that the difference of the multiplicities of ϕ on the two regions adjacent to the β curve stays positive. Proceeding along the handle until we reach the disk region, we again get $n_m > 0$. Thus in either case, we are done. \square

FIGURE 3.9. Local coefficients of ϕ at various points

4. USING $SFH(Y(R))$ TO DISTINGUISH SEIFERT SURFACES

Given an oriented knot $K \subset S^3$, there are several notions of equivalence one could consider for its Seifert surfaces. We will consider two Seifert surfaces, R_1, R_2 , to be *equivalent* if there is an isotopy of S^3 taking R_1 to R_2 . Note that this is the same as considering R_1 and R_2 to be equivalent if there is an orientation preserving diffeomorphism between the pairs (S^3, R_1) and (S^3, R_2) (since the group of orientation preserving diffeomorphisms of the three-sphere is path-connected). A more restrictive notion, called *strong equivalence*, regards R_1 and R_2 as equivalent if they are isotopic in the complement of K . Note that we can discuss whether the surfaces R_1 and R_2 are equivalent if ∂R_1 and ∂R_2 are equivalent knots, while we can say that two surfaces are strongly equivalent only if $\partial R_1 = \partial R_2$.

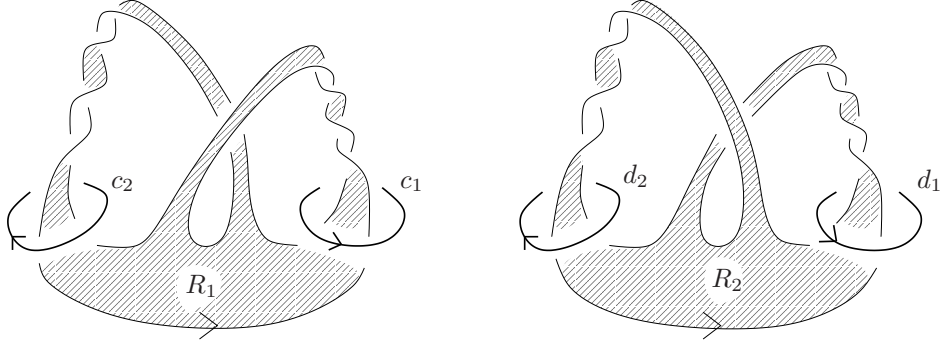


FIGURE 4.1. Two different Seifert surfaces for the same knot, 8_3 . The outward normal to each surface on the shaded region is out of the plane of the page (towards the reader).

The remainder of this section will be devoted to showing how the sutured Floer homology invariants of $S^3(R)$ can be used to distinguish non-equivalent Seifert surfaces. We do this through a detailed discussion of an example. Figure 4.1 depicts two Seifert surfaces, R_1 and R_2 , each bounded by the knot 8_3 . Note that R_1 is obtained by plumbing two bands with $+2$ and -2 full twists, respectively, and R_2 is obtained by taking the dual plumbing. So indeed the two surfaces bound the same oriented knot. We will show that R_1 and R_2 are inequivalent. Combining this with the results of [14], it will follow that these represent all isotopy classes of Seifert surface for 8_3 (see Proposition 4.3 below).

4.1. Classical Methods. Before beginning, we make some preliminary remarks regarding this particular example and the applicability of previously known techniques. As mentioned in the introduction, one effective way to distinguish isotopy classes of surfaces is through the fundamental group of their complements, see [1]. In the present case, however, this obviously fails. Indeed, $S^3 \setminus R_1$ is homeomorphic to $S^3 \setminus R_2$; they are both open handlebodies of genus 2. Thus any attempt to use the fundamental group will be fruitless.

Even in the case that the complements of the surfaces are homeomorphic, classical techniques could still be of use. The Seifert form provides a useful obstruction to finding an isotopy between two surfaces. To describe this, recall that $H_1(R; \mathbb{Z})$ is equipped with a bilinear form,

$$Q_R : H_1(R; \mathbb{Z}) \otimes H_1(R; \mathbb{Z}) \rightarrow \mathbb{Z},$$

called the Seifert form. Given curves a and b in R , let b^+ be a push-off of b in the direction specified by the positive unit normal vector field of R . Then the Seifert form evaluated on $([a], [b])$ is the linking number of a with b^+ in S^3 . Suppose now that two Seifert surfaces are isotopic. It follows that they have congruent Seifert forms. This means that there exists $W \in SL(2g, \mathbb{Z})$ for which

$$V_{R_2} = W^T V_{R_1} W,$$

where V_{R_i} are integral matrices representing Q_{R_i} with respect to given bases for $H_1(R_i; \mathbb{Z}) \cong \mathbb{Z}^{2g}$. Concretely, W is the matrix representing the isomorphism of $H_1(R; \mathbb{Z})$ induced by the diffeomorphism $(S^3, R_1) \cong (S^3, R_2)$. Thus, to show that two Seifert surfaces are inequivalent, it suffices to show that their Seifert forms are not congruent (see [30] for applications of this method to Seifert surfaces of some pretzel knots). In the situation at hand, however, this method also fails. For the obvious symplectic bases, the following matrices represent the Seifert forms of R_1 and R_2 :

$$V_{R_1} = \begin{pmatrix} 2 & 0 \\ 1 & -2 \end{pmatrix} \quad V_{R_2} = \begin{pmatrix} 2 & -1 \\ 0 & -2 \end{pmatrix}.$$

The intersection forms in the same basis are represented by

$$U_{R_1} = U_{R_2} = \begin{pmatrix} 0 & 1 \\ -1 & 0 \end{pmatrix}.$$

One can easily check, however, that V_{R_1} and V_{R_2} are congruent. An appropriate element of $SL(2, \mathbb{Z})$ is

$$W = \begin{pmatrix} 4 & -5 \\ -3 & 4 \end{pmatrix}.$$

Note that W also preserves the standard symplectic form on \mathbb{Z}^2 , i.e., $U_{R_2} = W^T U_{R_1} W$, so the Seifert form and the intersection form together are incapable of distinguishing R_1 and R_2 .

Finally, we remark that techniques from the theory of sutured manifolds have been quite fruitful in studying Seifert surfaces up to strong equivalence. See, for instance, [15, 14]. Indeed [14] has used these techniques to classify minimal genus Seifert surfaces up to strong equivalence for knots of 10 or fewer crossings. In particular, it follows that if R_1 and R_2 are dual plumbings of a $+2$ and a -2 twisted band, then they represent distinct strong equivalence classes, and that these are the only two such classes. It should be noted, however, that equivalence and strong equivalence are quite different. For instance, if the bands both had framing $+2$, then the boundary of the resulting dual surfaces would each be the knot 7_4 . It follows from [14] that these two surfaces are strongly inequivalent. It is easy to verify, however, that they are isotopic, and hence equivalent in our sense. As our techniques are able to distinguish surfaces up to isotopy, we will make no further reference to strong equivalence.

4.2. The Technique. Suppose that two surfaces R_1 and R_2 are isotopic. It follows that the complementary sutured manifolds, $S^3(R_1)$ and $S^3(R_2)$, will be equivalent. Thus to show that R_1 and R_2 are inequivalent, it suffices to show that the sutured Floer homology groups $SFH(S^3(R_1))$, $SFH(S^3(R_2))$ are different.

The algorithm from the previous section tells us how to construct Heegaard diagrams adapted to the surfaces. From these diagrams, we can identify generators for the chain complexes and determine the difference between the relative Spin^c structures associated to generators, \mathbf{x} and \mathbf{y} .

After analyzing the chain groups, we will determine their homology indirectly through consideration of the Euler characteristic. The total rank of the groups will agree for R_1 and R_2 , since it equals the rank of the top group of the knot Floer homology of $\partial R_i = 8_3$. Thus the heart of the argument is to distinguish the groups by showing that their Spin^c gradings are different.

Given $\mathfrak{s}_1, \mathfrak{s}_2 \in \underline{\text{Spin}}^c(S^3(R_i))$ which support non-trivial Floer groups, our analysis of the chain complexes will produce a geometric representative for the difference class $\text{PD}[\mathfrak{s}_1 - \mathfrak{s}_2] \in H_1(S^3 \setminus R_i; \mathbb{Z})$. To show that the Floer homology groups of $S^3(R_1)$ and $S^3(R_2)$ are different, we thus need a way to distinguish the various difference classes in $H_1(S^3 \setminus R_1; \mathbb{Z})$ from those in $H_1(S^3 \setminus R_2; \mathbb{Z})$. This is rather subtle, however, since the presentation for $H_1(S^3 \setminus R_i; \mathbb{Z})$ depends on the Heegaard diagram (or, equivalently, the presentation of R_i), and there could be an equivalence between $S^3(R_1)$ and $S^3(R_2)$ which induces an automorphism of $H_1(S^3 \setminus R; \mathbb{Z})$.

To remove this ambiguity we use the Seifert form of the surface. To describe this, let R be a Seifert surface for a knot $K \subset S^3$, and let $M = S^3 \setminus \text{Int}(R \times I)$ be the complement of a regular neighborhood of R . Then we have the following natural isomorphisms.

$$\begin{aligned}
H_1(R) &\cong H_1(R, \partial R) && \text{(Long exact sequence for the pair)} \\
&\cong H^1(R) && \text{(Poincaré Duality)} \\
&\cong H^2(S^3, R) && \text{(Long exact sequence for the pair)} \\
&\cong H^2(M, \partial M) && \text{(Excision)} \\
&\cong H_1(M). && \text{(Poincaré Duality)}
\end{aligned}$$

Since the Seifert form is invariant under isotopy of R , the above isomorphisms endow $H_1(M) \cong H_1(S^3 \setminus R)$ with a bilinear form which we also denote by Q_R . Given $a, b \in H_1(S^3 \setminus R; \mathbb{Z})$, let us denote $Q_R(a, b)$ by $a \cdot b$. Similarly, using the above isomorphisms, we can endow $H_1(S^3 \setminus R)$ with another bilinear form which is obtained from the intersection pairing on $H_1(R)$. Its value on the pair (a, b) will be denoted by $a \cap b$. The discussion shows that if $h: (S^3, R_1) \rightarrow (S^3, R_2)$ is an orientation preserving homeomorphism then $h_*: H_1(S^3 \setminus R_1) \rightarrow H_1(S^3 \setminus R_2)$ satisfies $a \cdot b = h_*(a) \cdot h_*(b)$ and $a \cap b = h_*(a) \cap h_*(b)$.

Let $\langle c_1, c_2 \rangle$ and $\langle d_1, d_2 \rangle$ be bases of $H_1(S^3 \setminus R_1)$ and $H_1(S^3 \setminus R_2)$, respectively, as shown on Figure 4.1. Tracing through the isomorphisms in our particular examples shows that matrix representations for Q_{R_i} are also given by the matrices V_{R_i} above. Thus $c_i \cdot c_j$ (resp. $d_i \cdot d_j$) is given by the ij -th entry of V_{R_i} . The values of $a \cdot b$ will distinguish the difference classes discussed above which, in turn, will distinguish the sutured Floer homology as relatively graded groups.

4.3. Calculation. Consider the two Seifert surfaces R_1, R_2 for 8_3 shown in Figure 4.1. In this section, we calculate the sutured Floer homology groups of $S^3(R_i)$, showing that $SFH(S^3(R_1)) \not\cong SFH(S^3(R_2))$. We discuss R_1 in detail, and then summarize the results for R_2 .

4.3.1. Drawing the diagram. Figures 4.2 and 4.3 illustrate the construction of the surface diagram for the first surface, R_1 . Our choice of basepoints ensures that the resulting B arc of $K = \partial R_1$ does not intersect the α curves. When removing the 3 intersections of the A arc with the β curves, we use only isotopies of the β curves. Thus the resulting surface diagram is extremal in the sense that we do not use any stabilizations in the algorithm from Subsection 3.2.

The bottom of Figure 4.3 shows the surface diagram, i.e., the Heegaard diagram for the sutured manifold $S^3_2(K)$ (the knot complement with 2 parallel meridional sutures) with R_1 appearing as a quasi-polygon.

At this point, it is straightforward to construct the sutured Heegaard diagram for $S^3(R_1)$. Simply remove the quasi-polygon representing R_1 from Σ (the shaded region labeled P in Figure 4.3), and glue two copies of it to what remains in such a way that the gluing is along A arcs on one copy and B arcs on the other. This is shown in Figure 4.4

After the decomposition, there are no intersection points of α and β curves lying on the two quasipolygons, P_A, P_B which we glued to $\Sigma \setminus P$. Thus, the 3-tuples of intersection points which comprise generators for the chain complex will be contained in $\Sigma \setminus P$. For that reason, it is convenient to erase all the β arcs which intersect P in the surface diagram of Figure 4.3. The resulting diagram is shown in Figure 4.5. This latter diagram is simpler to work with, in general, and contains the homotopy theoretic data necessary to understand the chain complex as a relatively $H_1(S^3 \setminus R_1)$ graded group.

4.3.2. The generators and their relative gradings. From Figure 4.5, we see that there are 10 generators for the sutured Floer chain complex. We can label these generators by triples, where $\mathbf{x} = x_1 x_2 x_3$ denotes the generator which contains the point labeled x_i on α_i . Given generators \mathbf{x} and \mathbf{y} , we wish to calculate the difference of their associated Spin^c structures, $\mathfrak{s}(\mathbf{x}) - \mathfrak{s}(\mathbf{y})$. To do this, join each x_i to y_i by an oriented arc along α_i , and then join y_i to some x_j by an oriented arc along a β curve. The result is a collection of closed

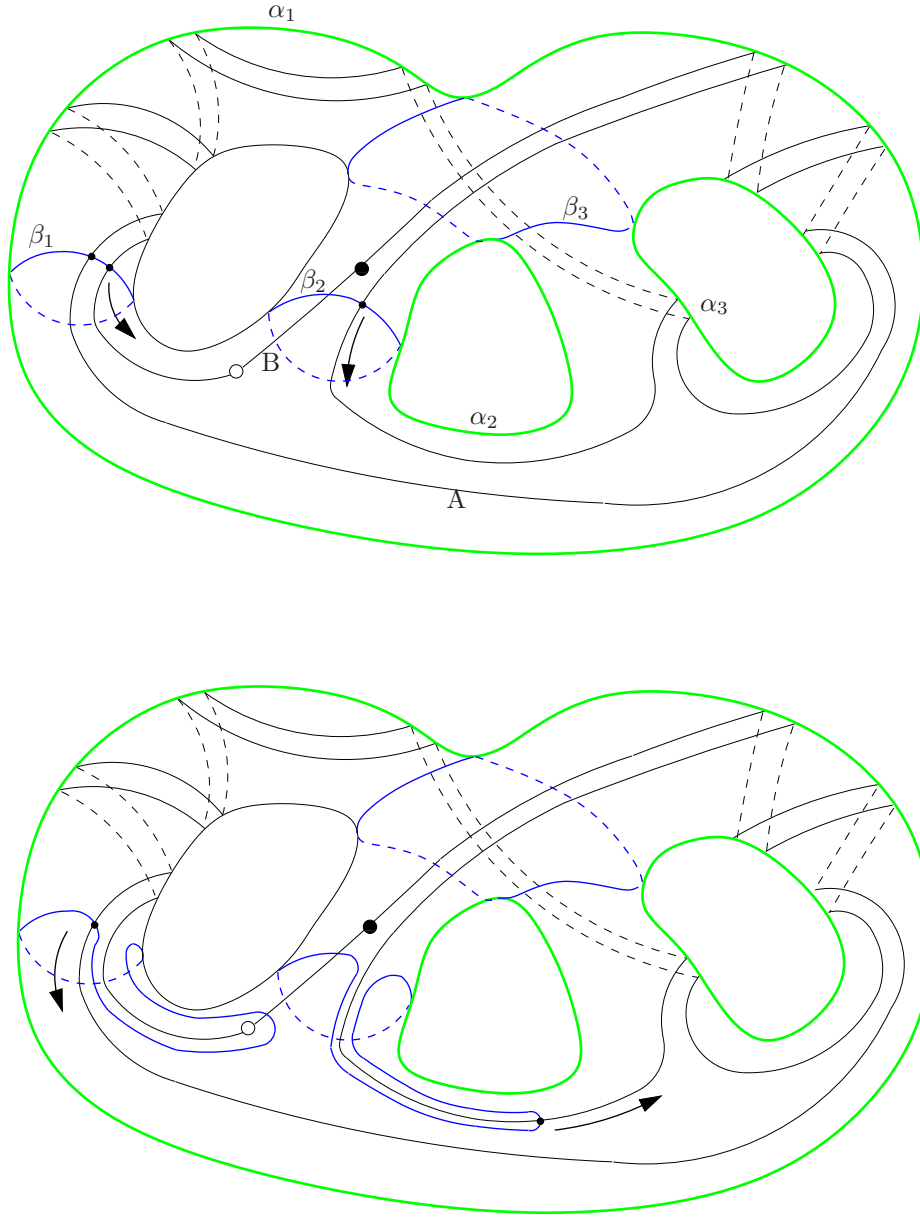


FIGURE 4.2. Constructing the surface diagram for R_1 . The first figure shows a Heegaard diagram for S^3 containing R_1 as a proper subsurface. The thick green curves are α_i , $i = 1, 2, 3$ while the thin blue curves are β_i , $i = 1, 2, 3$. There are three intersection points between the A arc and the β curves, which we remove by a sequence of isotopies.

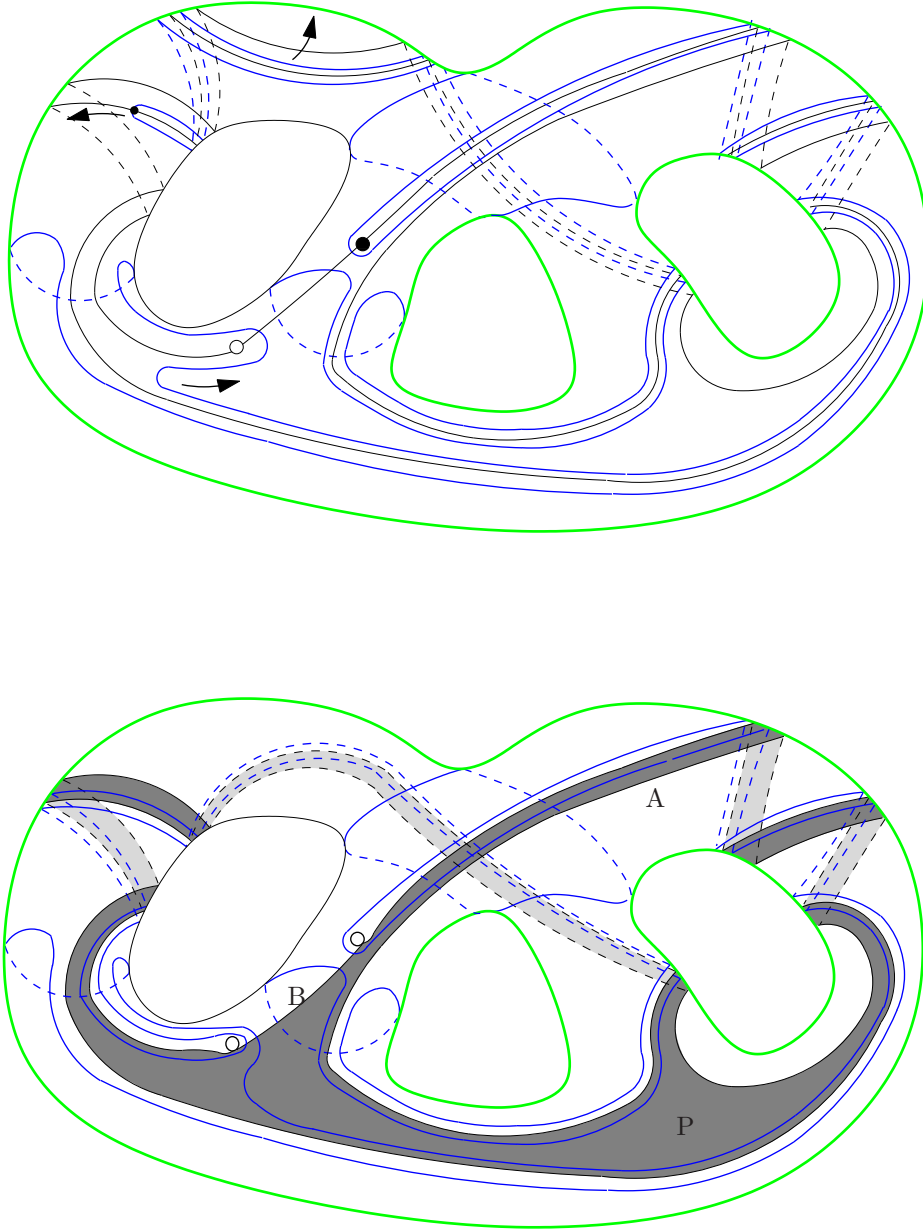


FIGURE 4.3. The bottom figure is the surface diagram for R_1 . We have shaded the quasi-polygon which represents $R_1 \subset S^3 \setminus K$.

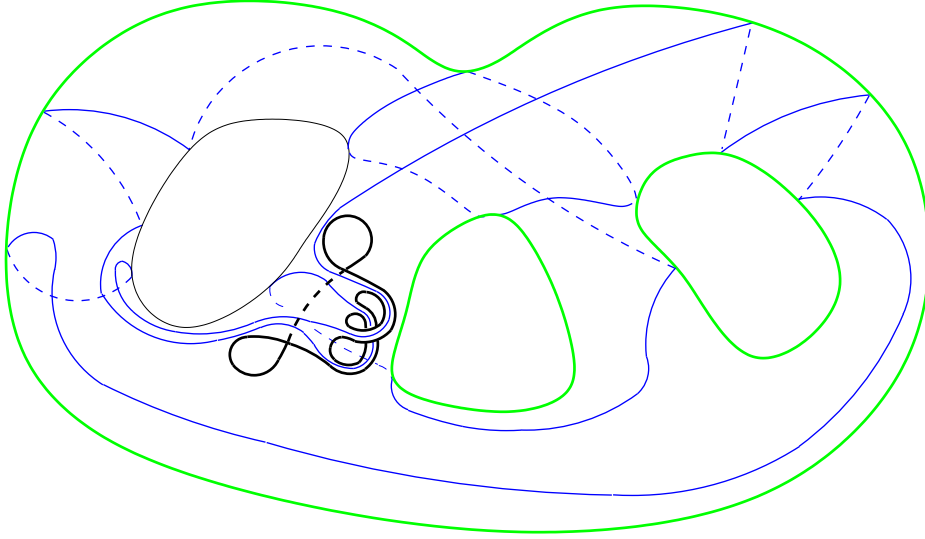


FIGURE 4.4. The decomposed diagram, i.e., the sutured diagram for $S^3(R_1)$. The bold curve is the boundary of the Heegaard surface.

curves, $\gamma_{\mathbf{x}, \mathbf{y}}$ whose homology class we denote by $\epsilon(\mathbf{x}, \mathbf{y}) = [\gamma_{\mathbf{x}, \mathbf{y}}] \in H_1(S^3 \setminus N(R_1); \mathbb{Z}) \cong H_1(S^3 \setminus R_1; \mathbb{Z})$, and refer to it as the *difference class* associated to \mathbf{x}, \mathbf{y} . According to Lemma 2.17, the class $\epsilon(\mathbf{x}, \mathbf{y})$ is Poincaré dual to $\mathfrak{s}(\mathbf{x}) - \mathfrak{s}(\mathbf{y}) \in H^2(S^3 \setminus N(R_1), \partial; \mathbb{Z})$. Note that since the β arcs in Figure 4.5 are connected, $\gamma_{\mathbf{x}, \mathbf{y}}$ can be taken to lie entirely in that figure. A cycle representative for the difference class of $\mathbf{x} = 512$ and $\mathbf{y} = 313$ is shown in Figure 4.6.

Ultimately, we wish to evaluate the Seifert form on the difference classes. To this end, it will be convenient to express $\epsilon(\mathbf{x}, \mathbf{y})$ in terms of the basis for $H_1(S^3 \setminus R_1; \mathbb{Z})$ given by c_1, c_2 in Figure 4.1. In order to do this, push the parts $\gamma_{\mathbf{x}, \mathbf{y}}$ which lie on the α arcs towards the α handlebody (i.e., outwards). Similarly, push the parts of $\gamma_{\mathbf{x}, \mathbf{y}}$ lying on the β curves towards the β handlebody (i.e., inwards). The result is a closed curve $\tilde{\gamma}_{\mathbf{x}, \mathbf{y}}$ which punctures the Heegaard surface only at the intersection points comprising \mathbf{x} and \mathbf{y} . See Figure 4.7. Note, however, that the Heegaard surface contains the presentation of the Seifert surface in Figure 4.1. Furthermore, $\tilde{\gamma}_{\mathbf{x}, \mathbf{y}}$ is in the complement of this presentation since the intersection points comprising \mathbf{x} and \mathbf{y} do not intersect the Seifert surface.

Thus we can regard $\tilde{\gamma}_{\mathbf{x}, \mathbf{y}}$ in two ways: as a curve in the sutured manifold $S^3(R_1)$ presented by the decomposed diagram or as a curve in the complement of R_1 , as shown in Figure 4.1. We claim that the homology class which $\tilde{\gamma}_{\mathbf{x}, \mathbf{y}}$ represents in $H_1(S^3 \setminus R_1)$ is the same, regardless of which way we view it. In this way, we can determine the difference classes in terms of the basis for $H_1(S^3 \setminus R_1)$ given by c_1, c_2 in Figure 4.1.

To prove the claim, one need only trace through the construction of the sutured diagram, starting from the presentation of R_1 in Figure 4.1. We began by constructing a diagram for S^3 which contained R_1 as a subsurface (the top part of Figure 4.2). Regarding $\tilde{\gamma}_{\mathbf{x}, \mathbf{y}}$ on this diagram, its homology class clearly agrees with that obtained by thinking of it as a curve in Figure 4.1. Indeed, removing β_1 and β_2 from this diagram specifies $S^3 \setminus R_1$ as it is presented in Figure 4.1 (see Remark 3.1). It follows that isotopies of β_1, β_2 do not change the homology class of $\tilde{\gamma}_{\mathbf{x}, \mathbf{y}}$ in $S^3 \setminus R_1$. The surface diagram differs from the diagram for S^3 containing R_1 only by a sequence of isotopies, followed by the removal of two disks to turn it into a sutured diagram for

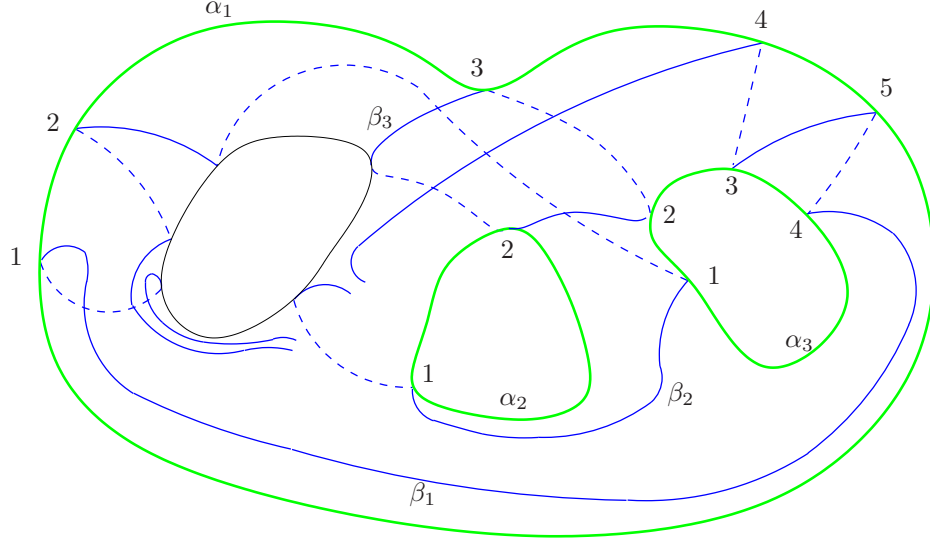


FIGURE 4.5. The surface diagram from Figure 4.3, where we have erased all arcs of intersection $\beta \cap P$ of the β curves with the quasipolygon P representing R_1 . This diagram contains all 3-tuples of intersection points $\alpha_i \cap \beta_{\sigma(i)}$ which comprise the generators of $SFH(S^3(R_1))$.

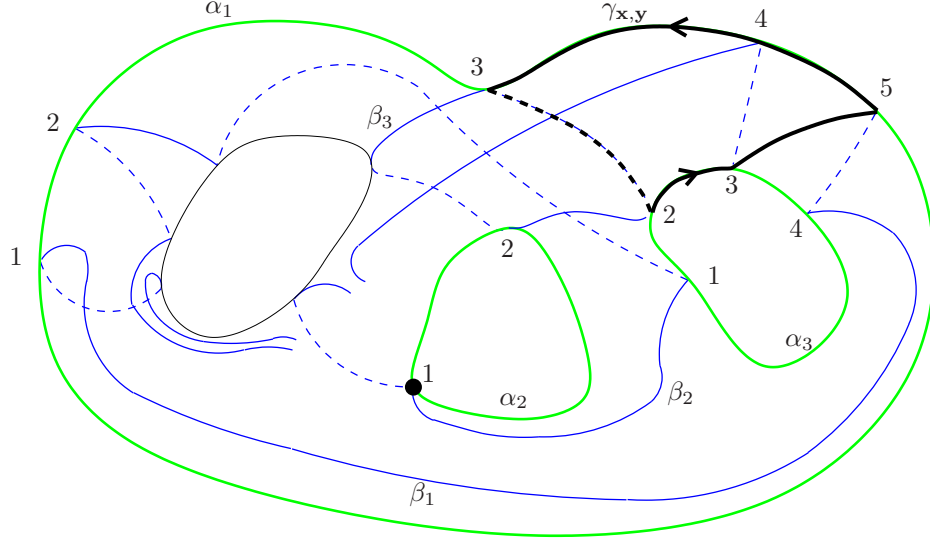


FIGURE 4.6. Construction of a cycle representative, γ , of the difference class, $\epsilon(\mathbf{x}, \mathbf{y}) = \text{PD}[\mathfrak{s}(\mathbf{x}) - \mathfrak{s}(\mathbf{y})] \in H_1(S^3 \setminus R_1)$. Here $\mathbf{x} = 512$, $\mathbf{y} = 313$. The representative is comprised of two curves, one of which is constant at $1 \in \alpha_2 \cap \beta_2$.

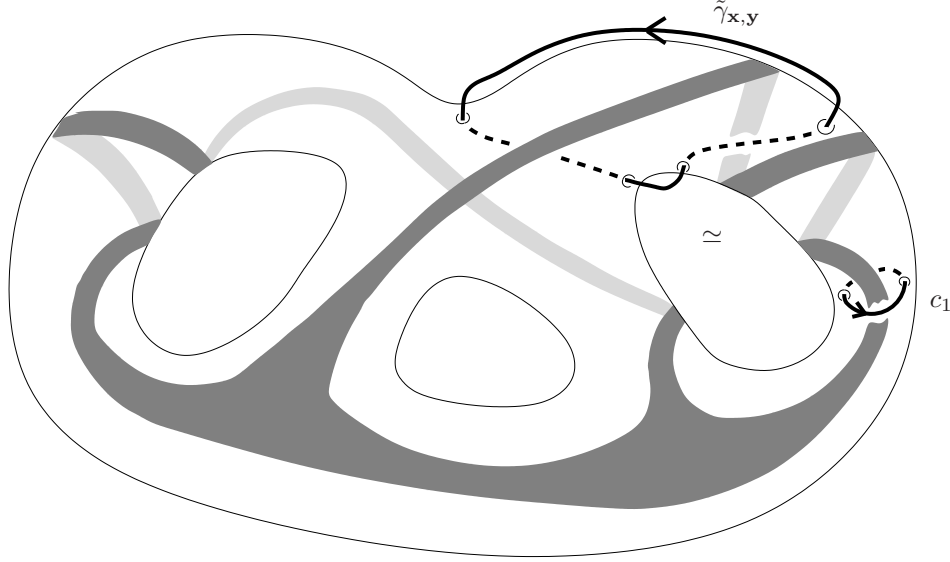


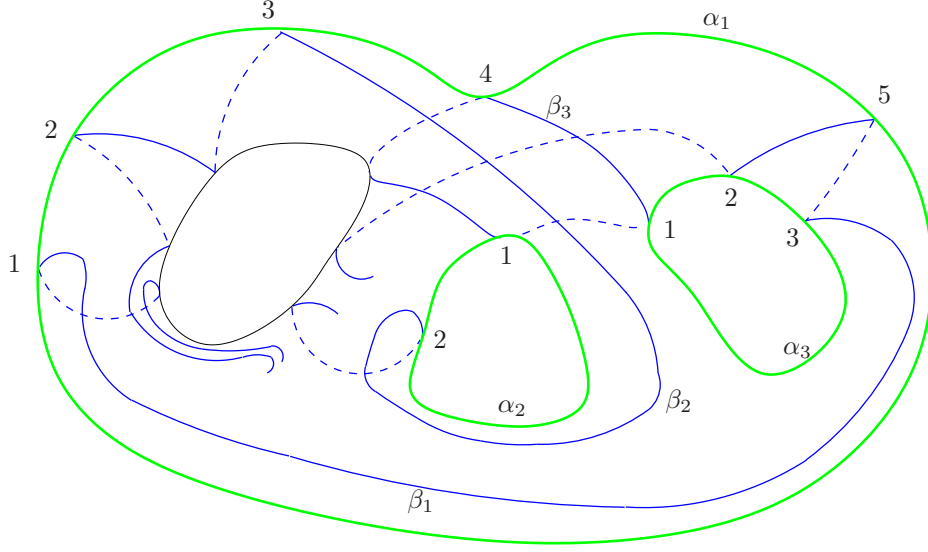
FIGURE 4.7. The push-off of $\gamma_{\mathbf{x},\mathbf{y}}$ into the handlebodies yields a curve $\tilde{\gamma}_{\mathbf{x},\mathbf{y}}$ living in the complement of R_1 . In this example, $\tilde{\gamma}_{\mathbf{x},\mathbf{y}}$ is homologous to c_1 .

$S_2^3(K)$. This latter modification, however, is performed far from $\tilde{\gamma}_{\mathbf{x},\mathbf{y}}$ and hence does not effect its homology class. Another way to see this is that the surface diagram, by definition, specifies an embedding of the Seifert surface in the knot complement $S^3 \setminus K$. From its construction, this embedding differs from the embedding shown in Figure 4.1 only by an isotopy supported in an arbitrarily small neighborhood of ∂R_1 . Thus, the homology class of $\tilde{\gamma}_{\mathbf{x},\mathbf{y}}$ in $H_1(S^3 \setminus R_1)$ specified by the surface diagram agrees with that of Figure 4.1. Finally, decomposing the diagram is exactly the same as decomposing $S_2^3(K)$. Since $\tilde{\gamma}_{\mathbf{x},\mathbf{y}}$ is in the complement of the quasipolygon, its homology class in $H_1(S^3 \setminus R_1)$ (as specified by the Heegaard diagram) is unchanged by the decomposition. This proves the claim.

Figures 4.6 and 4.7 indicate that the difference class between $\mathbf{x} = 512$ and $\mathbf{y} = 313$ is c_2 . The remaining differences are easily computed, and the following diagram represents the chain complex as a relatively $H_1(S^3 \setminus R_1)$ graded group. (The explanation for the diagram is that each \mathbf{x} is placed on a lattice point in the affine lattice generated by c_1, c_2 . The difference between the lattice coordinates of \mathbf{x} and \mathbf{y} is the difference class $\epsilon(\mathbf{x}, \mathbf{y})$.)

$$\begin{array}{ccccc}
 223 & \xrightarrow{c_1} & 224 & & \\
 \downarrow c_2 & & \downarrow c_2 & & \\
 313, 412, 421 & \xrightarrow{c_1} & 314, 512, 521 & \xrightarrow{c_1} & 112, 121
 \end{array}$$

4.3.3. The homology. We take our chain complexes with $\mathbb{Z}/2\mathbb{Z}$ coefficients. Our first observation is that the rank of the homology of the chain complex above is 4. This follows from Theorem 2.20 above, together with the fact that $\text{rk } \widehat{HFK}(K, 1) = 4$. This latter fact can be seen in many ways and follows, for instance from the fact that 8_3 is an alternating knot of genus 1 for which the top coefficient of the Alexander polynomial

FIGURE 4.8. Diagram for R_2 .

equals -4 . (According to Theorem 1.3 of [21], for alternating knots, one has

$$\text{rk } \widehat{HFK}(K, i) = |a_i|,$$

where a_i is the i -th coefficient of the symmetrized Alexander polynomial $\Delta_K(T) = a_0 + \sum_i a_i(T^i + T^{-i})$.) Now the homology of each of the 2 subcomplexes in the top row of the diagram is $\mathbb{Z}/2\mathbb{Z}$; indeed, each complex has a single generator. This takes care of a 2-dimensional subspace of the 4-dimensional homology. As for the rest of the homology, note that the subcomplex generated by 112, 121 must have even Euler characteristic while the subcomplexes generated by 314, 512, 521 and 313, 412, 421, respectively have odd (in particular, non-zero) Euler characteristics. The only way for this to happen is if the 112, 121 subcomplex is acyclic and the homology of the remaining two subcomplexes is $\mathbb{Z}/2\mathbb{Z}$. Summarizing, the sutured Floer homology as a relatively $H_1(S^3 \setminus R_1)$ graded group is

$$\begin{array}{ccc} \mathbb{Z}/2\mathbb{Z} & \xrightarrow{c_1} & \mathbb{Z}/2\mathbb{Z} \\ \downarrow c_2 & & \downarrow c_2 \\ \mathbb{Z}/2\mathbb{Z} & \xrightarrow{c_1} & \mathbb{Z}/2\mathbb{Z} \end{array}$$

4.3.4. *The results for R_2 .* Figure 4.8 shows the Heegaard diagram for R_2 . The resulting chain complex has 8 generators, whose relative gradings are given in terms of the basis d_1, d_2 of Figure 4.1 as follows

$$\begin{array}{ccc}
 212 & \xrightarrow{d_1} & 213 \\
 \downarrow d_2 & & \downarrow d_2 \\
 312 & \xrightarrow{d_1} & 313 \\
 \downarrow d_2 & & \downarrow d_2 \\
 422, 521 & \xrightarrow{d_1} & 423, 121
 \end{array}$$

As above, the rank of the sutured Floer homology for $S^3(R_2)$ is 4. Since the Euler characteristic of the subcomplexes generated by $422, 521$ and $423, 121$ are even, the sutured Floer homology is given by

$$\begin{array}{ccc}
 \mathbb{Z}/2\mathbb{Z} & \xrightarrow{d_1} & \mathbb{Z}/2\mathbb{Z} \\
 \downarrow d_2 & & \downarrow d_2 \\
 \mathbb{Z}/2\mathbb{Z} & \xrightarrow{d_1} & \mathbb{Z}/2\mathbb{Z}
 \end{array}$$

4.3.5. *Distinguishing the groups.* Having calculated the sutured Floer homology of $S^3(R_1)$ and $S^3(R_2)$ as relatively graded groups, it remains to distinguish them.

We first remind the reader what it means for two collections of groups graded by relative Spin^c structures to be isomorphic.

Definition 4.1. Two relative Spin^c -graded groups

$$SFH(M_1, \gamma_1) = \bigoplus_{\mathfrak{s} \in \underline{\text{Spin}}^c(M_1, \gamma_1)} SFH(M_1, \gamma_1, \mathfrak{s}) \quad , \quad SFH(M_2, \gamma_2) = \bigoplus_{\mathfrak{s} \in \underline{\text{Spin}}^c(M_2, \gamma_2)} SFH(M_2, \gamma_2, \mathfrak{s})$$

are *isomorphic* (which we denote $SFH(M_1, \gamma_1) \cong SFH(M_2, \gamma_2)$) if

- (1) There is an isomorphism, $f^* : H^2(M_1, \partial M_1; \mathbb{Z}) \rightarrow H^2(M_2, \partial M_2; \mathbb{Z})$.
- (2) There is a bijection of sets $\sigma : \underline{\text{Spin}}^c(M_1, \gamma_1) \rightarrow \underline{\text{Spin}}^c(M_2, \gamma_2)$.
- (3) The following diagram commutes

$$\begin{array}{ccc}
 \underline{\text{Spin}}^c(M_1, \gamma_1) \times H^2(M_1, \partial M_1; \mathbb{Z}) & \xrightarrow{(\sigma, f^*)} & \underline{\text{Spin}}^c(M_2, \gamma_2) \times H^2(M_2, \partial M_2; \mathbb{Z}) \\
 \downarrow & & \downarrow \\
 \underline{\text{Spin}}^c(M_1, \gamma_1) & \xrightarrow{\sigma} & \underline{\text{Spin}}^c(M_2, \gamma_2)
 \end{array}$$

where the vertical arrows are induced by the action of $H^2(M_i, \gamma_i)$ on $\underline{\text{Spin}}^c(M_i, \gamma_i)$.

- (4) There are isomorphisms $g_{\mathfrak{s}} : SFH(M_1, \gamma_1, \mathfrak{s}) \rightarrow SFH(M_2, \gamma_2, \sigma(\mathfrak{s}))$ for every $\mathfrak{s} \in \underline{\text{Spin}}^c(M_1, \gamma_1)$.

If $f : (M_2, \gamma_2) \rightarrow (M_1, \gamma_1)$ is an equivalence, then Theorem 2.16 indicates that $SFH(M_1, \gamma_1) \cong SFH(M_2, \gamma_2)$. In this case, f^* and σ in Definition 4.1 are both obtained by pull-back along f . In addition, if f comes from the restriction of an equivalence of Seifert surfaces $(S^3, R_2) \rightarrow (S^3, R_1)$, then $f_* : H_1(S^3 \setminus R_1) \rightarrow H_1(S^3 \setminus R_2)$ preserves the Seifert form discussed in Subsection 4.2, i.e., $a \cdot b = f_*(a) \cdot f_*(b)$.

Returning to our example, this can be made concrete as follows. Let us denote generators for the 4 non-zero Floer homology groups of R_1 (resp. R_2) by \mathbf{x}_i (resp. \mathbf{y}_i), so that the Floer homology groups are given by

$$\begin{array}{ccc}
\langle \mathbf{x}_2 \rangle & \xrightarrow{c_1} & \langle \mathbf{x}_1 \rangle \\
\downarrow c_2 & & \downarrow c_2 \\
\langle \mathbf{x}_4 \rangle & \xrightarrow{c_1} & \langle \mathbf{x}_3 \rangle
\end{array}
\qquad
\begin{array}{ccc}
\langle \mathbf{y}_2 \rangle & \xrightarrow{d_1} & \langle \mathbf{y}_1 \rangle \\
\downarrow d_2 & & \downarrow d_2 \\
\langle \mathbf{y}_4 \rangle & \xrightarrow{d_1} & \langle \mathbf{y}_3 \rangle
\end{array}$$

where, $\langle - \rangle$ means the $\mathbb{Z}/2\mathbb{Z}$ vector space generated by $-$. Then, in order for $SFH(S^3(R_1))$ to be isomorphic to $SFH(S^3(R_2))$, there must be a bijection between sets

$$\sigma : \{\mathbf{x}_1, \mathbf{x}_2, \mathbf{x}_3, \mathbf{x}_4\} \longrightarrow \{\mathbf{y}_1, \mathbf{y}_2, \mathbf{y}_3, \mathbf{y}_4\},$$

which is compatible with taking difference classes, i.e., $\epsilon(\sigma(\mathbf{x}_i), \sigma(\mathbf{x}_j)) = f_*\epsilon(\mathbf{x}_i, \mathbf{x}_j)$, for some isomorphism $f_* : H_1(S^3 \setminus R_1) \rightarrow H_1(S^3 \setminus R_2)$. Since we assume that R_1 is equivalent to R_2 , f_* must preserve the Seifert form.

Suppose that σ exists. Then we have

$$\epsilon(\sigma(\mathbf{x}_1), \sigma(\mathbf{x}_2))^2 = f_*\epsilon(\mathbf{x}_1, \mathbf{x}_2)^2 = \epsilon(\mathbf{x}_1, \mathbf{x}_2)^2 = c_1^2 = 2,$$

where squares indicate the pairing, under the Seifert form, of a class with itself. Thus the difference of $\sigma(\mathbf{x}_1)$ and $\sigma(\mathbf{x}_2)$ is a class whose square is 2. Considering $\epsilon(\mathbf{y}_i, \mathbf{y}_j)$ for every $i \neq j$, we obtain 8 distinct classes

$$\pm d_1 \qquad \pm d_2 \qquad \pm(d_1 + d_2) \qquad \pm(d_1 - d_2),$$

whose squares are

$$2 \qquad -2 \qquad -1 \qquad 1,$$

respectively. This shows that $\epsilon(\sigma(\mathbf{x}_1), \sigma(\mathbf{x}_2)) = \pm d_1$. Similarly, the fact that

$$\epsilon(\sigma(\mathbf{x}_1), \sigma(\mathbf{x}_3))^2 = f_*\epsilon(\mathbf{x}_1, \mathbf{x}_3)^2 = \epsilon(\mathbf{x}_1, \mathbf{x}_3)^2 = c_2^2 = -2,$$

implies that $\epsilon(\sigma(\mathbf{x}_1), \sigma(\mathbf{x}_2)) = \pm d_2$. We have arrived at a contradiction. For on the one hand

$$\epsilon(\sigma(\mathbf{x}_1), \sigma(\mathbf{x}_2)) \cdot \epsilon(\sigma(\mathbf{x}_1), \sigma(\mathbf{x}_3)) = \epsilon(\mathbf{x}_1, \mathbf{x}_2) \cdot \epsilon(\mathbf{x}_1, \mathbf{x}_3) = c_1 \cdot c_2 = 0,$$

while on the other we have shown

$$\epsilon(\sigma(\mathbf{x}_1), \sigma(\mathbf{x}_2)) \cdot \epsilon(\sigma(\mathbf{x}_1), \sigma(\mathbf{x}_3)) = \pm d_1 \cdot \pm d_2,$$

and this latter pairing is non-zero, regardless of signs. This shows that $SFH(S^3(R_1)) \not\cong SFH(S^3(R_2))$, and hence $R_1 \not\sim R_2$.

Remark 4.2. Our argument shows that there does not exist an orientation-preserving diffeomorphism of S^3 which takes R_1 to R_2 . There is, however, an obvious orientation-reversing diffeomorphism which sends R_1 to R_2 . To see this, simply reflect R_1 across the plane of the page, then rotate 180° around a vertical axis through the middle of the surface. The composition of the reflection and rotation is the aforementioned diffeomorphism. Our result, then, can be interpreted as saying that sutured Floer homology detects “chirality” of Seifert surfaces. On the other hand, it is an interesting fact that the knot 8_3 is fully amphichiral.

4.4. A few consequences.

Proposition 4.3. *R_1 and R_2 represent all equivalence classes of minimal genus Seifert surfaces for 8_3 .*

Proof. By [14] the knot 8_3 has exactly two Seifert surfaces up to strong equivalence, namely R_1 and R_2 . We have just seen above that these two surfaces are inequivalent. The result follows. \square

Theorem 4.4. *For any $n \geq 1$, there exists a knot K_n with Seifert surfaces $\{F_0, \dots, F_n\}$, such that F_i is not equivalent to F_j for any $i \neq j$.*

Proof. Take K_n to be the connected sum of n copies of 8_3 , and let F_i be the Seifert surface obtained by forming the boundary connected sum of i copies of R_1 and $n-i$ copies of the R_2 . Note that we can perform $n-1$ product disk decompositions⁴ to $S^3(F_i)$ to obtain a sutured manifold which is equivalent to the disjoint union of i copies of $S^3(R_1)$ and $n-i$ copies of $S^3(R_2)$. Now sutured Floer homology is unchanged under product decompositions (see Lemma 9.13 of [10]), and under disjoint union behaves according to the Künneth principle:

$$SFH(Y_1 \sqcup Y_2, \gamma_1 \sqcup \gamma_2, \mathfrak{s}_1 \sqcup \mathfrak{s}_2) \cong SFH(Y_1, \gamma_1, \mathfrak{s}_1) \otimes SFH(Y_2, \gamma_2, \mathfrak{s}_2).$$

(where we work with $\mathbb{Z}/2\mathbb{Z}$ coefficients to avoid any Tor terms). Using these facts together with the calculation from the previous section, we can distinguish the number of copies of R_1 used to form F_i as follows. First, observe that $\text{rk } SFH(S^3(F_i)) = 4^n$. A generating set for the Floer homology of F_i is given by n -tuples $\mathbf{x}_j \mathbf{y}_m$, with $\mathbf{j} = \{j_1, \dots, j_i\}$, $\mathbf{m} = \{m_1, \dots, m_{n-i}\}$ and $j_l, m_k \in \{1, 2, 3, 4\}$. The n -tuple $\mathbf{x}_j \mathbf{y}_m$ corresponds to

$$\mathbf{x}_{j_1}^1 \otimes \dots \otimes \mathbf{x}_{j_i}^i \otimes \mathbf{y}_{m_1}^1 \otimes \dots \otimes \mathbf{y}_{m_{n-i}}^{n-i},$$

where $\mathbf{x}_{j_l}^l$ (resp. $\mathbf{y}_{j_l}^l$) is one of the 4 generators of the sutured Floer homology of the l -th copy of R_1 (resp. R_2) used to form F_i . The difference classes associated to the generators are then given by

$$\epsilon(\mathbf{x}_j \mathbf{y}_m, \mathbf{x}_{j'} \mathbf{y}_{m'}) = \epsilon(\mathbf{x}_{j_1}, \mathbf{x}_{j'_1}) \oplus \dots \oplus \epsilon(\mathbf{x}_{j_i}, \mathbf{x}_{j'_i}) \oplus \epsilon(\mathbf{y}_{m_1}, \mathbf{y}_{m'_1}) \oplus \dots \oplus \epsilon(\mathbf{y}_{m_{n-i}}, \mathbf{y}_{m'_{n-i}}),$$

with $\epsilon(\mathbf{x}_{j_l}, \mathbf{x}_{j'_l})$ (resp. $\epsilon(\mathbf{y}_{j_l}, \mathbf{y}_{j'_l})$) one of the 8 distinct differences $\pm c_1^l, \pm c_2^l, \pm(c_1^l + c_2^l), \pm(c_1^l - c_2^l)$ (resp. $\pm d_1^l, \pm d_2^l, \pm(d_1^l + d_2^l), \pm(d_1^l - d_2^l)$). Here, as throughout, the upper indices on c_k^l (resp. d_k^l) are used to denote an element in $H_1(S^3 \setminus F_i)$ which comes from the l -th copy of R_1 (resp. R_2). Finally, we note that the Seifert form on $H_1(S^3(F_i)) \cong \mathbb{Z}^{2n}$ splits as a sum,

$$Q_{F_i} = Q_{R_1^1} \oplus \dots \oplus Q_{R_1^i} \oplus Q_{R_2^1} \oplus \dots \oplus Q_{R_2^{n-i}}.$$

Now suppose that F_i is isotopic to F_k for some $i \neq k$. As in the previous section, this implies that there is a bijection between generators

$$\sigma : \{\mathbf{x}_j \mathbf{y}_m\} \rightarrow \{\tilde{\mathbf{x}}_j \tilde{\mathbf{y}}_m\},$$

which is compatible with an isomorphism $f_* : H_1(S^3 \setminus F_i) \rightarrow H_1(S^3 \setminus F_k)$, which preserves the Seifert form. We use \sim to distinguish generators for F_k from those for F_i . Abusing notation, for $k \in \mathbb{Z}$ let $\mathbf{k} = \{k, k, \dots, k\}$ denote the vector of any length, all of whose entries are k . We have

$$\epsilon(\sigma(\mathbf{x}_1 \mathbf{y}_1), \sigma(\mathbf{x}_2 \mathbf{y}_2))^2 = f_* \epsilon(\mathbf{x}_1 \mathbf{y}_1, \mathbf{x}_2 \mathbf{y}_2)^2 = \epsilon(\mathbf{x}_1 \mathbf{y}_1, \mathbf{x}_2 \mathbf{y}_2)^2 = (c_1^1 + \dots + c_1^i + d_1^1 + \dots + d_1^{n-i})^2 = 2n.$$

It follows that

$$\epsilon(\sigma(\mathbf{x}_1 \mathbf{y}_1), \sigma(\mathbf{x}_2 \mathbf{y}_2)) = \delta_1 c_1^1 + \dots + \delta_k c_1^k + \rho_1 d_1^1 + \dots + \rho_{n-k} d_1^{n-k},$$

for some choice of signs $\delta_l, \rho_l \in \{-1, 1\}$. Indeed these are the only elements in $H_1(S^3 \setminus F_k)$ of square $2n$ which arise as differences of generators. A similar analysis shows that

$$\epsilon(\sigma(\mathbf{x}_1 \mathbf{y}_1), \sigma(\mathbf{x}_3 \mathbf{y}_3)) = \delta'_1 c_2^1 + \dots + \delta'_k c_2^k + \rho'_1 d_2^1 + \dots + \rho'_{n-k} d_2^{n-k},$$

as these are the only elements in $H_1(S^3 \setminus F_k)$ of square $-2n$. We claim that the signs must agree in both cases; that is, $\delta'_l = \delta_l$ and $\rho'_l = \rho_l$ for all l . To see this observe that f_* , in addition to preserving the Seifert form, must preserve the intersection product on $H_1(S^3 \setminus F_i)$ inherited from $H_1(F_i)$ (equivalently, f_* must be a symplectomorphism of the symplectic vector space $H_1(S^3 \setminus F_i; \mathbb{R})$). Denoting this product by \cap , we have

$$\epsilon(\mathbf{x}_1 \mathbf{y}_1, \mathbf{x}_2 \mathbf{y}_2) \cap \epsilon(\mathbf{x}_1 \mathbf{y}_1, \mathbf{x}_3 \mathbf{y}_3) = (c_1^1 + \dots + c_1^i + d_1^1 + \dots + d_1^{n-i}) \cap (c_2^1 + \dots + c_2^i + d_2^1 + \dots + d_2^{n-i}) = n.$$

⁴A product disk decomposition is a surface decomposition along a properly embedded disk which intersects the sutures in exactly 2 points.

On the other hand,

$$\begin{aligned} \epsilon(\sigma(\mathbf{x}_1\mathbf{y}_1), \sigma(\mathbf{x}_2\mathbf{y}_2)) \cap \epsilon(\sigma(\mathbf{x}_1\mathbf{y}_1), \sigma(\mathbf{x}_3\mathbf{y}_3)) &= f_*\epsilon(\mathbf{x}_1\mathbf{y}_1, \mathbf{x}_2\mathbf{y}_2) \cap f_*\epsilon(\mathbf{x}_1\mathbf{y}_1, \mathbf{x}_3\mathbf{y}_3) = \\ &= (\delta_1 c_1^1 + \cdots + \delta_k c_1^k + \rho_1 d_1^1 + \cdots + \rho_{n-k} d_1^{n-k}) \cap (\delta'_1 c_2^1 + \cdots + \delta'_k c_2^k + \rho'_1 d_2^1 + \cdots + \rho'_{n-k} d_2^{n-k}) = \\ &\quad \delta_1 \delta'_1 c_1^1 \cap c_2^1 + \cdots + \delta_k \delta'_k c_1^k \cap c_2^k + \rho_1 \rho'_1 d_1^1 \cap d_2^1 + \cdots + \rho_{n-k} \rho'_{n-k} d_1^{n-k} \cap d_2^{n-k} = \\ &\quad = \delta_1 \delta'_1 + \cdots + \delta_k \delta'_k + \rho_1 \rho'_1 + \cdots + \rho_{n-k} \rho'_{n-k}, \end{aligned}$$

and this latter expression can equal n only when $\delta'_l = \delta_l$ and $\rho'_l = \rho_l$ for all l . This proves the claim.

To complete the proof of the theorem, calculate

$$\epsilon(\mathbf{x}_1\mathbf{y}_1, \mathbf{x}_2\mathbf{y}_2) \cdot \epsilon(\mathbf{x}_1\mathbf{y}_1, \mathbf{x}_3\mathbf{y}_3) = c_1^1 \cdot c_2^1 + \cdots + c_1^i \cdot c_2^i + d_1^1 \cdot d_2^1 + \cdots + d_1^{n-i} \cdot d_2^{n-i} = i - n.$$

Since f_* preserves the Seifert form this should be equal to

$$\begin{aligned} \epsilon(\sigma(\mathbf{x}_1\mathbf{y}_1), \sigma(\mathbf{x}_2\mathbf{y}_2)) \cdot \epsilon(\sigma(\mathbf{x}_1\mathbf{y}_1), \sigma(\mathbf{x}_3\mathbf{y}_3)) &= \\ &= \delta_1 \delta'_1 c_1^1 \cdot c_2^1 + \cdots + \delta_k \delta'_k c_1^k \cdot c_2^k + \rho_1 \rho'_1 d_1^1 \cdot d_2^1 + \cdots + \rho_{n-k} \rho'_{n-k} d_1^{n-k} \cdot d_2^{n-k} = k - n. \end{aligned}$$

Since $i \neq k$, the proof is complete. \square

5. DIRECTIONS FOR FUTURE RESEARCH

As our intent was to introduce the tools necessary for the study of Seifert surfaces through sutured Floer homology, there are many directions one could pursue and questions left unanswered.

One interesting aspect of our particular examples was that the sutured Floer homology groups contained no more information than their Euler characteristic. Indeed, while the Euler characteristic of sutured Floer homology was not a previously studied invariant, it is classical in the sense that it is an appropriate version of Turaev torsion. On the one hand, this tells us that there is a useful invariant of Seifert surfaces which exists independent of Floer homology (and is easier to compute). On the other, it begs the question to find examples where the full power of the Floer homology is needed. Of course taking the connected sum of our examples with the unique minimal genus Seifert surface of a Whitehead doubled knot will produce examples of Seifert surfaces distinguished by sutured Floer homology groups whose Euler characteristic is trivial, but presumably these case could still be handled by “classical” techniques.

In another direction, we have a computable invariant which can presumably be used to start the isotopy classification of minimal genus Seifert surfaces for knots in the tables (recall, again, that the previous classifications were for the somewhat less natural notion of strong equivalence). Since little appears to be known generally about this type of equivalence, filling in the tables may be a useful first step.

Finally, in analogy with the Ozsváth-Szabó knot invariants, it seems reasonable to ask if there are geometric or combinatorial properties of Seifert surfaces (perhaps having an alternating projection) which constrain the sutured Floer invariants.

REFERENCES

1. W. R. Alford, *Complements of minimal spanning surfaces of knots are not unique*, Ann. of Math. **91** (1970), no. 2, 419–424.
2. G. Burde and H. Zieschang, *Neuwirthsche knoten und flächenabbildungen*, Abh. Math. Sem. Univ. Hamburg **31** (1967), 239–246.
3. J. R. Eisner, *Knots with infinitely many minimal spanning surfaces*, Trans. Amer. Math. Soc. **229** (1977), 329–349.
4. D. Gabai, *Foliations and the topology of 3-manifolds*, J. Differential Geom. **18** (1983), 445–503.
5. ———, *The Murasugi sum is a natural geometric operation*, Contemp. Math. **20** (1983), 131–143.
6. ———, *Detecting fibred links in S^3* , Comment. Math. Helv. **61** (1986), no. 4, 519–555.
7. ———, *Foliations and the topology of 3-manifolds II*, J. Differential Geom. **26** (1987), 461–478.
8. P. Ghiggini, *Knot Floer homology detects genus-one fibred knots*, Amer. J. Math. (to appear, available at math.GT/0603445).

9. A. Juhász, *The sutured Floer homology polytope*, math.GT/0802.3415.
10. ———, *Holomorphic discs and sutured manifolds*, Algebr. Geom. Topol. **6** (2006), 1429–1457.
11. ———, *Floer homology and surface decompositions*, Geom. Topol. **12** (2008), 299–350.
12. ———, *Knot Floer homology and Seifert surfaces*, Algebr. Geom. Topol. **8** (2008), 603–608.
13. O. Kakimizu, *Finding disjoint incompressible spanning surfaces for a link*, Hiroshima Math. J. **22** (1992), 225–236.
14. ———, *Classification of the incompressible spanning surfaces for prime knots of 10 or less crossings*, Hiroshima Math. J. **35** (2005), no. 1, 47–92.
15. T. Kobayashi, *Uniqueness of minimal genus Seifert surfaces for links*, Topology Appl. **33** (1989), no. 3, 265–279.
16. R. Lipshitz, *A cylindrical reformulation of Heegaard Floer homology*, Geom. Topol. **10** (2006), 955–1097.
17. H. C. Lyon, *Simple knots without unique minimal surfaces*, Proc. A.M.S. **43** (1974), no. 2, 449–454.
18. C. Manolescu, P. Ozsváth, and S. Sarkar, *A combinatorial description of knot Floer homology*, math.GT/0607691.
19. Y. Ni, *Sutured Heegaard diagrams for knots*, Algebr. Geom. Topol. **6** (2006), 513–537.
20. ———, *Knot Floer homology detects fibred knots*, Invent. Math. **170** (2007), no. 3, 577–608.
21. P. Ozsváth and Z. Szabó, *Heegaard Floer homology and alternating knots*, Geom. Topol. **7** (2003), 225–254.
22. ———, *Holomorphic disks and 3-manifold invariants: properties and applications*, Ann. of Math. **159** (2004), no. 3, 1159–1245.
23. ———, *Holomorphic disks and genus bounds*, Geometry and Topology **8** (2004), 311–334.
24. ———, *Holomorphic disks and knot invariants*, Adv. Math. **186** (2004), no. 1, 58–116.
25. ———, *Holomorphic disks and topological invariants for closed three-manifolds*, Ann. of Math. **159** (2004), no. 3, 1027–1158.
26. ———, *Holomorphic disks and topological invariants for closed three-manifolds*, Ann. of Math. (2) **159** (2004), no. 3, 1027–1158.
27. J. A. Rasmussen, *Floer homology and knot complements*, PhD thesis, Harvard University (2003).
28. S. Sarkar and J. Wang, *An algorithm for computing some Heegaard Floer homologies*, math.GT/0607777.
29. W. P. Thurston, *A norm for the homology of 3-manifolds*, Mem. Amer. Math. Soc. **59** (1986), i–vi & 99–130.
30. H. F. Trotter, *Some knots spanned by more than one unknotted surface of minimal genus*, Knots, groups, and 3-manifolds (Papers dedicated to the memory of R. H. Fox), Princeton Univ. Press, 1975, pp. 51–63.
31. V. Turaev, *Torsion invariants of spin^c -structures on 3-manifolds*, Math. Res. Lett. **4** (1997), 679–695.